EFFECT OF PIEZOELECTRIC ACTUATOR PLACEMENT ON CONTROLLING THE MODES OF VIBRATION FOR FLEXIBLE STRUCTURES

BY

Khaled S. Al Athel

A Thesis Presented to the

DEANSHIP OF GRADUATE STUDIES

KING FAHD UNIVERSITY OF PETROLEUM & MINERALS

DHAHRAN, SAUDI ARABIA

In Partial Fulfillment of the
Requirements for the Degree of

MASTER OF SCIENCE

In

MECHANICAL ENGINEERING

July 2005

KING FAHAD UNIVERSITY OF PETROLEUM & MINERALS

DHAHRAN 31261, SAUDI ARABIA

DEANSHIP OF GRADUATE STUDIES

This thesis, written by Khaled Saleh Al-Athel, under the direction of his thesis advisor and approved by his thesis committee, has been presented to and accepted by the Dean of Graduate Studies, in partial fulfillment of the requirements for the degree of MASTER OF SCIENCE IN MECHANICAL ENGINEERING.

Thesis Committee

Dr. Mehmet Sunar
Thesis Advisor

Dr. Yehia Khulief
Member

Dr. Saif Al-Kaabi
Member

Dr. Faleh Al-Sulaiman
ME Department Chairman

Dr. Mohammad Al-Ohali
Dean of Graduate Studies

١٤٢٦/٥/٢٩

Date 6-7-2005

DEDICATION

To all of those who had faith in me

To Dr. Saleh Al-Athel, my father, who was always supporting me and helping me throughout all my years in school and college

To Dr. M. Sunar, my thesis advisor, who helped me in my thesis and taught me many things in the area of Dynamics & Control

To Dr. A. Arif, who got me interested in the area of Finite Element Method and supported me through my Master's program

To all my family

And finally, to my wife for supporting me and believing in me

ACKNOWLEDGMENT

Acknowledgment is due to the King Fahad University of Petroleum & Minerals for supporting this research.

I wish to express my appreciation to Dr. M. Sunar who served as my thesis advisor and helped me a lot in my research. I also wish to thank my thesis committee members Dr. S. Al-Kaabi and Dr. Y. Khuleif for the help and comments I got from them to present this work in its final form.

TABLE OF CONTENTS

LIST OF TABLES

LIST OF FIGURES

THESIS ABSTRACT

Khaled Saleh Al-Athel

Thesis title: "EFFECT OF PIEZOELECTRIC ACTUATOR PLACEMENT ON CONTROLLING THE MODES OF VIBRATION FOR FLEXIBLE STRUCTURES"

Field: Mechanical Engineering

Date: July 2005

Vibration control is a large area of interest either in all sections of industry or in research. One way to control the vibration of dynamic systems is by using piezoelectric materials (PZT's). PZT's have been used to reduce vibration in both active and passive control systems and that is due to their special characteristics. In this work, the effect of the PZT actuator location on controlling the vibrations is studied. Two structures are used in the study, a 2-D beam and a 3-D plate with two different control techniques, an LQR controller and an LQG controller. The modeling is done using the well known finite element method. Results were found by simulating the cases in MATLAB. Validation of the results is done in ANSYS.

ملخص الرسالة

خالد صالح العذل

عنوان الرسالة: " تأثير وضعية مشغل الكهرباء الاجهادية على القدرة للتحكم في اطوار اهتزازات الإنشائات المرنة "

التخصص: الهندسة الميكانيكية

تاريخ التخرج: جمادى الثاني ١٤٢٦

التحكم بالاهتزازات يعتبر حاليا واحد من اهم مجالات الهندسة سواء في القطاع الـصناعي او فـي مجال الابحاث. استخدام المواد ذات الكهرباء الاجهادية, يعتبر واحد من الطرق المهمة في التحكم في الانظمة الديناميكية. تستخدم المواد ذات الكهرباء الاجهادية لتقليص الاهتزازات في مختلف انواع انظمة التحكم و ذلك بسبب خواصها الفريدة. في هذه الرسالة, تأثير وضعية مشغل الكهرباء الاجهادية على القـدرة للـتحكم فـي الاهتزازات سوف يشرح و يفصل. نوعان من المنشآت سوف يستخدمان في هذه الرسالة, عارضـة ثنائيـة الابعاد و صفيحة ثلاثية الابعاد. لكل منشأة نوعان من طرق التحكم سوف تستخدم, الاول هو منظم مـتحكم خطي ثنائي و الثاني هو قاوسيان متحكم خطي ثنائي. البرمجة في هذه الرسالة تمت باستخدام طرق العناصر المنتهية. النتائج اوجدت عن طريق المحاكاة باستخدام برنامج MATLAB. مقارنة النتائج و التأكد منها تـم عن طريق برنامج ANSYS.

CHAPTER 1

INTRODUCTION

Vibration control is an important area of interest in several industrial applications. Unwanted vibration can have a detrimental and some times catastrophic effect on the serviceability or structural integrity of mechanical systems. To control the vibrations in a system, different techniques have been developed. Some of these techniques and methods use piezoelectric materials as sensors or actuators.

Active control systems are required in applications where passive vibration control is not possible because of material constraints or simply not sufficient for the level of control required. Active control is a favorable method of control because it works in a wide frequency range, reducing resonant vibrations within that range and because it is adaptive to changes in the nature of the disturbance.

1.1 LITERATURE SURVEY

Piezoelectric materials have a very large scope of use in active control applications due to their ability to act as either sensors or actuators. An active control system reduces vibration by sensing and counteracting the undesired disturbance using the PZT sensors and actuators. There are different kinds of piezoelectric

materials. Piezopolymers are usually used as sensors, while piezoceramics are used as both sensors and actuators [19].

Piezoelectricity relates electric field with mechanical stress/strain in piezoelectric materials. Piezoelectric actuators have many advantages: (i) No moving parts and no friction will limit the lifetime by wear. (ii) The actuator requires electrical energy only during the expansion process. As soon as the desired position is reached no more electrical energy is needed to maintain this position. (iii) Almost infinite small positioning ability. (iv) Piezoelectric actuators can be used as high-speed translators. (v) Large masses can be moved and positioned accurately using piezoelectric actuators [16].

Using piezoelectric materials in control applications has proved that they are very good in controlling the vibrations. Adaptive structures using piezoelectric materials are usually called smart structures.

Jacques and Pierre Curie, two French physicists, were the first to discover the piezoelectric effect back in 1880 [20]. Originally specially shaped crystals of natural minerals, quartz in particular, were used. Now, the manufactured ceramics are the most commonly used piezoelectric materials.

Due to their special characteristics, the piezoelectric materials have been utilized extensively in precision control of dynamical systems. Crawley and de Luis

of MIT [5] were among the first researchers to use the piezoelectric materials as elements of an intelligent structure. They introduced an analytical model and they compared it with an experimental set. They performed a scaling analysis to demonstrate that the effectiveness of piezoelectric actuators is independent of the size of the structure and to evaluate various piezoelectric materials based on their effectiveness in transmitting strain to the substructure. Another pioneer in this field, Tzou of University of Kentucky [6], developed a light weight robot end-effecter using piezoelectric materials.

Using a piezoelectric actuator in a fixed position, the first two modes of vibration for a beam were controlled by Bayon and Hanagud [1]. They used a single actuator to suppress vibrations by using acceleration feedback controllers. Knowing the frequencies for a smart structure helps in designing the parameters of a controller. Different approaches to estimate the multi-modal frequencies for a smart structure were done using the real time analysis [3].

Using piezoelectric materials as actuators and sensors, the base acceleration can be reconstructed by the sensory capabilities of the piezoelectric ceramics and especially developed reconstruction filters. In this way the forces occurring in the structure can be reduced by about a factor of 20 [4].

A test procedure and a control strategy regarding the actuator and sensor placement were done numerically by Wodek Gawronski. The study did not include the dynamics of the actuator and the sensor in the modeling of the structure [7].

Since many numerical analyses of smart structures are carried out, different control techniques are used to control the vibrations. Employing an LQ (linear quadratic) controller in a tracking system showed good results in controlling the vibrations in a cantilever beam [2].

1.2 CURRENT STATUS

Many researches on the control area uses PZT's as elements of the structure. The effect of these PZT's on the structure and the controller has not been discussed in details. The use of the PZT's as actuators is done, and the effect of the PZT's on the controller has been studied for a fixed location of the actuator. The next step is to study the effect of the PZT actuator location on the structure and the controller for different structures, actuator locations and control techniques.

1.3 OBJECTIVE OF THIS STUDY

In this thesis, the effect of the piezoelectric actuator placement on controlling the vibration of flexible structures will be studied. The study is carried out for a 2-D

beam and a 3-D plate. Two types of controllers will be investigated for their suitability in controlling the vibration of the structure, the first one is an LQR (Linear Quadratic Regulator) controller and the second one is an LQG (Linear Quadratic Gaussian) controller. The system, including the structure and the piezoelectric sensor and actuator, will be modeled through the well-known finite element method (FEM).

For each case, beam and plate, the models will be compared between MATLAB and ANSYS to check our FE formulations. The output voltages due to a unit step force will be compared between the two models.

Modal nodes will be checked for the actuator placement to ensure that the actuator node where we will feed the input voltages is not placed at any modal nodes. This will be done for the first three mode shapes for the beam, and for th first seven mode shapes for the plate.

This work produces a comprehensive study for the PZT actuator placement effect on controlling the structural vibrations. Also a full 3-D model, including the dynamics of the PZT's, with two types of controllers, LQR and LQG, will be done.

CHAPTER 2

PIEZOELECTRIC EQUATIONS

The coupled electromechanical behavior of piezoelectric medium can be described with adequate accuracy by linearized constitutive equations. These linear piezoelectric equations are used to study the behaviors of both the piezoelectric sensors and actuators.

Assuming that the mechanical and electrical forces are balanced at any time, the general form of the linear piezoelectric equations is written as [11]:

$$\begin{aligned} D &= e^t S + \varepsilon E \\ T &= cS - eE \end{aligned} \tag{2.1}$$

where,

D: vector of electrical displacement (charge per unit area),

$\boldsymbol{T}$: stress vector,

$\boldsymbol{S}$: strain vector,

$\boldsymbol{E}$: vector of the electric field,

e: piezoelectric constant matrix,

ε: dielectric matrix at constant strain, and

c: elasticity matrix at constant electric field.

The relations for the mechanical and electrical fields in the piezoelectric medium are as follows [11]:

$$\begin{aligned} S &= Lu \\ E &= -\nabla \phi \end{aligned} \tag{2.2}$$

Where L is a differential operator relating the strain vector $\boldsymbol{S}$ to the displacement vector $\boldsymbol{u}$, and ϕ is the electrical potential.

To derive the dynamic equation of the system, an energy functional Π is defined as:

$$\Pi = \int_V H dV - \int_V u^T P_b dV - \int_{S_1} u^T P_s dS - u^T P_c + \int_{S_2} \phi \sigma dS \tag{2.3}$$

Where H is the energy density defined as [12]:

$$H = \frac{1}{2} S^T cS - \frac{1}{2} E^T \varepsilon E - S^T eE \tag{2.4}$$

$\boldsymbol{P_b}$ and $\boldsymbol{P_s}$ are the respective vectors of body and surface forces applied to the volume V and surface S_1. Also, $\boldsymbol{P_c}$ is the vector of the concentrated forces and σ is the surface charge at surface S_2.

Using Hamilton's principle with the finite element approximation, one can obtain the dynamic finite element equations of the piezoelectric media. The Hamilton's principle is expressed as:

$$\delta\int_{t_1}^{t_2}(T-\Pi)\,dt=0 \tag{2.5}$$

Where the kinetic energy T can be given as:

$$T=\frac{1}{2}\int_V \rho\dot{\mathbf{u}}^T\dot{\mathbf{u}}dV \tag{2.6}$$

Where ρ is the mass density, $\dot{u}$ is the velocity vector. Now using (2.6), equation (2.5) can be re-written as:

$$\delta\int_{t_1}^{t_2}\Pi dt=\delta\int_{t_1}^{t_2}Tdt=-\int_{t_1}^{t_2}\int_V \rho\delta u^T\ddot{u}dVdt \tag{2.7}$$

Upon using integration by parts with proper boundary conditions for the energy density H, it can be shown that

$$\delta H=\delta S^T T-\delta E^T D \tag{2.8}$$

The finite element approximation, in general form, for the displacement and the electric potential are written as:

$$\begin{aligned} \boldsymbol{u}_{el} &= N_u u_i \\ \boldsymbol{\phi}_{el} &= N_\phi \boldsymbol{\phi}_i \end{aligned} \tag{2.9}$$

Where $\boldsymbol{u}_{el}$ and $\boldsymbol{\phi}_{el}$ are the displacement vector and the electrical potential pertaining to the finite element. In equation (2.9), u_i and $\boldsymbol{\phi}_i$ are the nodal displacement and electrical potential vectors, and N_u and N_ϕ are the shape function matrices for the displacement and electrical fields, respectively. Accordingly, Eq. (2.2) can be re-written as:

$$\begin{aligned} S_{el} &= \left[L \; N_u \right] u_i = B_u u_i \\ E_{el} &= -\left[\nabla \; N_\phi \right] \boldsymbol{\phi}_i = -B_\phi \boldsymbol{\phi}_i \end{aligned} \tag{2.10}$$

Using Eq. (2.10) with Eq. (2.5) gives the dynamic equations for the piezoelectric medium after the assemblage:

$$M_{uu}\ddot{\boldsymbol{u}} + K_{uu}\boldsymbol{u} + K_{u\phi}\boldsymbol{\phi} = \boldsymbol{F} \tag{2.11}$$

$$K_{\phi u}\,\boldsymbol{u} - K_{\phi\phi}\boldsymbol{\phi} = \boldsymbol{G} \tag{2.12}$$

Where $\boldsymbol{u}, \boldsymbol{\phi}$, $\boldsymbol{F}$ and $\boldsymbol{G}$ are the global nodal displacement, electric potential, force and applied charge vectors, respectively. The matrices and vectors for the finite element in equations (2.11) and (2.12) are found as follows:

$$\left[M_{uu}\right]_{el}=\int_{V_{el}} \rho N_u^T N_u \, dV \,, \quad \left[K_{u\phi}\right]_{el}=\int_{V_{el}} B_u^T e B_\phi \, dV$$

$$\left[K_{uu}\right]_{el}=\left[\int_{V_{el}} B_u^T c B_u \, dV\right], \quad \left[K_{\phi\phi}\right]_{el}=\int_{V_{el}} B_\phi^T \varepsilon B_\phi \, dV \tag{2.13}$$

$$\boldsymbol{G_{el}}=-\int_{(S_2)_{el}} N_\phi^T \sigma dS \,, \qquad \boldsymbol{F_{el}}=\int_{V_{el}} N_u^T \boldsymbol{P_b} dV+\int_{(S_1)_{el}} N_u^T \boldsymbol{P_s} dS + N_u^T \boldsymbol{P_c}$$

Since there is no applied charge at the piezoelectric sensor, that is $\boldsymbol{G} = \boldsymbol{0}$ for the sensor layer, the sensor output can be written from Eq. (2.12) as:

$$\phi = K_{\phi\phi}^{-1} K_{\phi u} \boldsymbol{u} \tag{2.14}$$

The relation between the applied voltage and the charge for is given by:

$$G = c_p V \tag{2.15}$$

Where c_p is the piezoelectric material capacitance. Substituting equations (2.12) and (2.15) into Eq. (2.11) gives the equation for the actuator layer as:

$$M_{uu}\ddot{\boldsymbol{u}} + C_{uu}\dot{\boldsymbol{u}} + [\,K_{uu} + K_{u\phi}K_{\phi\phi}^{-1}K_{\phi u}\,]\,\boldsymbol{u} = \boldsymbol{F} + c_p K_{u\phi} K_{\phi\phi}^{-1} \boldsymbol{V} \tag{2.16}$$

Where C_{uu} is the proportional damping matrix assumed to be:

$$C_{uu} = \alpha M_{uu} + \beta K_{uu} \tag{2.17}$$

Where α and β are the Rayleigh's coefficients.

In Eq. (2.16), the voltage can be used as the feedback voltage to the actuator layer. The input to the controller is taken as the time derivative of the output of the piezoelectric sensor ($\dot{\phi}$) and the output of the controller is fed back to the piezoelectric actuator (***V***). Assuming a negative feedback law for the controller and using Eq. (2.14), the feedback voltage to the actuator is obtained as:

$$V = -K\dot{\phi} = -KK_{\phi\phi}^{-1}K_{\phi u}\dot{u} \tag{2.18}$$

Where K is the constant feedback gain matrix that can be determined for different types of controllers.

Using Eq. (2.18) in Eq. (2.16) yields the equation of motion for the closed loop system as

$$M_{uu}\ddot{\boldsymbol{u}} + [C_{uu} + c_p K_{u\phi}K_{\phi\phi}^{-1}KK_{\phi\phi}^{-1}K_{\phi u}]\dot{\boldsymbol{u}} + [K_{uu} + K_{u\phi}K_{\phi\phi}^{-1}K_{\phi u}]\boldsymbol{u} = \boldsymbol{F} \tag{2.19}$$

For linear control methods in state space such as LQR, LQG and H_∞, the equation of motion should be written in state space form. To convert Eq. (2.16) into state space form, the force and feedback voltage vectors are first written as:

$$\begin{aligned} F &= D_f f \\ V &= D_v v \end{aligned} \tag{2.20}$$

Where D_f and D_v are the position matrices for the force and voltage. Now, Eq. (2.16) is expressed in state space form as:

$$\begin{aligned} \dot{z} &= A z + B v \\ y &= C z + D v \end{aligned} \tag{2.21}$$

where A, B, C and D are the state, actuator input, system output and direct transmission matrices, and $\boldsymbol{z}$ and $\boldsymbol{y}$ are the state and system output vectors. The state vector **z** and matrices A and B are found as:

$$\boldsymbol{z}=\begin{bmatrix} \boldsymbol{u} \\ \dot{\boldsymbol{u}} \end{bmatrix},\ A=\begin{bmatrix} 0 & I \\ -M_{uu}^{-1}K_{uu}^{*} & -M_{uu}^{-1}C_{uu} \end{bmatrix},\ B=\begin{bmatrix} 0 \\ M_{uu}^{-1}c_p K_{u\phi}K_{\phi\phi}^{-1}D_v \end{bmatrix} \tag{2.22}$$

Where I is the identity matrix, and K_{uu}^{*} is defined as:

$$K_{uu}^{*} = K_{uu} + K_{u\phi}K_{\phi\phi}^{-1}K_{\phi u} \tag{2.23}$$

The LQR and LQG laws can be applied to Eq. (2.21) to find the optimum gain matrix K. A PID controller can also be designed using either Eq. (2.16) or (2.21).

CHAPTER 3

BEAM WITH PZT ACTUATOR AND SENSOR

3.1 PROBLEM DEFINITION

In this chapter, a simple smart system containing a clamped beam instrumented with a PZT sensor and a PZT actuator is tested for vibration control (Figure 3.1). The length, width and depth of the beam are taken as 0.08, 0.001 and 0.016 m, respectively. For the PZT sensor and actuator, the length, width and depth are taken as 0.01, 0.0004 and 0.016 m, respectively. The material properties are listed in Table 3.1.

Figure 3.1 Smart system consisting of beam, PZT sensor and PZT actuator.

TABLE 3.1 Material Properties for the beam with PZT's

Piezoceramic (BM500) [13].	
c_{11} (Pa)	1.26×10^{11}
c_{12} (Pa)	8.41×10^{10}
c_{22} (Pa)	1.17×10^{11}
c_{33} (Pa)	1.26×10^{11}
e_{21} (C/m^2)	-5.4
e_{22} (C/m^2)	15.8
ε_{11} (F/m)	1.151×10^{-3}
ε_{22} (F/m)	1.043×10^{-3}
ρ (kg/m^3)	7800
Beam (St)	
Y (Pa)	2.07×10^{11}
ν	0.3
ρ (kg/m^3)	7800

The effect of the actuator placement on controlling the vibration of the beam will be tested using numerical simulations. The location of the sensor will be fixed throughout the simulations, where the actuator will be placed at different locations.

In our case study, two types of controllers will be used to study the effect of the actuator placement. The first one will be an LQR controller, and the second will be an LQG controller. In both cases, a unit step force will be applied in positive vertical direction at the tip of the beam.

3.2 MODELING

The smart system containing the beam and the PZT's will be modeled using the finite element method. The PZT's are modeled based on the linear piezoelectric equations discussed in chapter 1. The finite element equations for the beam are derived as follows: (Euler Beam)

To derive the beam finite element equations, the energy functional Π is taken as,

$$\Pi = \int_V \frac{1}{2} S_{xx}^T Y \; S_{xx} dV - \int_V \boldsymbol{u}^T \boldsymbol{P_b} \, dV - \int_S \boldsymbol{u}^T \boldsymbol{P_s} \, dV - \boldsymbol{u}^T \boldsymbol{P_c} \tag{3.1}$$

$$= \sum_{el} \int_{V_{el}} \frac{1}{2} S_{xx}^T Y_{el} \; S_{xx} dV - \sum_{el} \int_{V_{el}} \boldsymbol{u}_{el}^T \boldsymbol{P}_{\boldsymbol{b}el} \, dV - \sum_{el} \int_{S_{el}} \boldsymbol{u}_{el}^T \boldsymbol{P}_{s\,el} \, dV - \sum_{el} \boldsymbol{u}_{el}^T \boldsymbol{P}_{\boldsymbol{c}\,el}$$

where Y_{el} is the Young's modulus of elasticity and S_{xx} is the normal strain in x-direction given as

$$S_{xx} = -y\frac{d^2 v_{el}}{dx^2}. \tag{3.2}$$

where v_{el} is the transverse displacement of the beam element in y-direction. Hence, the first elemental integral in equation (3.1) becomes

$$\int_{V_{el}} \frac{1}{2} S_{xx}^T Y_{el} S_{xx} dV = \int_{A_{el}} y^2 dA \int_0^L \frac{Y_{el}}{2} \left(\frac{d^2 v_{el}}{dx^2}\right)^T \left(\frac{d^2 v_{el}}{dx^2}\right) dx = I_{el} \frac{Y_{el}}{2} \int_0^L \left(\frac{d^2 v_{el}}{dx^2}\right)^T \left(\frac{d^2 v_{el}}{dx^2}\right) dx \tag{3.3}$$

where $I_{el} = \int_{A_{el}} y^2 dA$ and L are the area moment of inertia and length of the beam element, respectively. For the finite element modeling, let

$$v_{el} = N_B \, \boldsymbol{u_i} \tag{3.4}$$

where the nodal displacement vector u_i is of 4th order containing the transverse displacements and slopes at both ends of the beam. In equation (3.4), the shape function matrix N_B is defined as

$$N_B = [N_{B1} \;\; N_{B2} \;\; N_{B3} \;\; N_{B4}] \tag{3.5}$$

where the Hermitian shape functions are used as

$$N_{B1}= \frac{1}{L^3}\left(2x^3 - 3x^2L + L^3\right), \quad N_{B2} = \frac{1}{L^3}\left(x^3L - 2x^2L^2 + xL^3\right)$$

$$N_{B3} = \frac{1}{L^3}\left(-2x^3 + 3x^2L\right), \quad N_{B4} = \frac{1}{L^3}\left(x^3L - x^2L^2\right). \tag{3.6}$$

In view of equation (3.4),

$$\frac{d^2v_{el}}{dx^2} = \frac{d^2N_B}{dx^2}\,\boldsymbol{u_i} = B_u\,\boldsymbol{u_i}. \tag{3.7}$$

Substituting equation (3.7) in equation (3.3) yields

$$\int_{V_{el}} \frac{1}{2}\, S_{xx}^T Y_{el}\; S_{xx} dV = I_{el}\,\frac{Y_{el}}{2}\int_0^L \boldsymbol{u_i}^T\; B_u^T\; B_u \boldsymbol{u_i}\; dx \tag{3.8}$$

whose variation becomes

$$\delta\left(I_{el}\,\frac{Y_{el}}{2}\int_0^L \boldsymbol{u_i}^T\; B_u^T\; B_u \boldsymbol{u_i}\; dx\right) = \boldsymbol{u_i}^T\; Y_{el} I_{el} \int_0^L B_u^T\; B_u\; dx\; \delta\boldsymbol{u_i}. \tag{3.9}$$

Hence the elemental stiffness matrix for the beam element is defined as

$$[K_{uu}]_{el} = Y_{el} I_{el} \int_0^L B_u^T\; B_u\; dx\;. \tag{3.10}$$

The elemental mass matrix $[M_{uu}]_{el}$ and force vector $\boldsymbol{F_{el}}$ for the beam element are defined similar to equations (2.12)

$$[M_{uu}]_{el} = \int_{V_{el}} \rho_{el} N_B^T N_B \, dV$$

$$\boldsymbol{F_{el}} = \int_{V_{el}} N_B^T \boldsymbol{P_{bel}} \, dV + \int_{S_{el}} N_B^T \boldsymbol{P_{sel}} \, dS + N_B^T \boldsymbol{P_{cel}} \ . \qquad (3.11)$$

Based on the beam and PZT's equations, an FE program is written in MATLAB. The beam is meshed into 20 elements, where the actuator and sensor are meshed into 4 elements each.

The Beam is considered to have three DOF, two translational and one rotational. The PZT's have three DOF, two translational and one is volt. Note that the PZT's are grounded at the boundary with beam, which means that the voltages are taken to be zero. Hence, the system has a total of 80 mechanical DOF (the node where the beam is fixed has zero DOF), and 10 electrical DOF. Figure 3.2 shows the model in the way it is meshed. Beam elements are 5 mm each, where PZT are 2.5 mm square elements. Note that at the boundary with the PZT's, beam elements are meshed with a size of 2.5 mm each

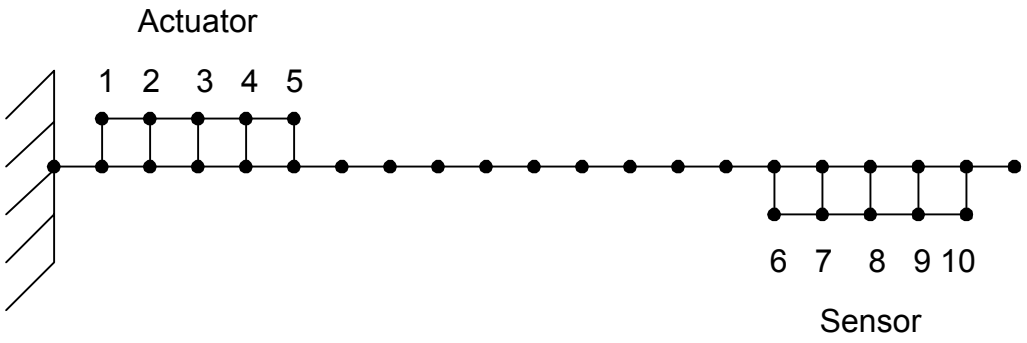

Figure 3.2 Finite element mesh of the beam & PZT's system (1)

Before we start the study, we should check the validation of the FE formulations. The model will be done using commercial FE software (ANSYS), and the sensor voltage output will be compared as obtained from MATLAB and ANSYS.

In ANSYS, the beam is modeled with a 2-D elastic beam element (BEAM3), and the PZT actuator and sensor are modeled using a 2-D coupled field element (PLANE13). Material properties are taken as in Table 3.1. Figure 3.3 shows the FE model used for the validation in MATLAB and ANSYS. Note that each PZT element is 5 mm square.

In both models, MATLAB and ANSYS, a unit step force is applied in the positive vertical direction at the tip of the beam. The voltages at nodes 7 and 9 of the sensor are plotted for MATLAB and ANSYS in Figures 3.4 and 3.5. As we can see that the difference between the sensor voltage outputs in ANSYS and MATLAB are acceptable. It is also clear that there is some shift between the two signals, and that

shift increases as we move with time. The reason for that is because there is some difference between the fundamental frequencies for both outputs. Table 3.2 shows the values for the first three natural frequencies obtained from MATLAB and ANSYS. From this point we can start the study with the model we did in MATLAB.

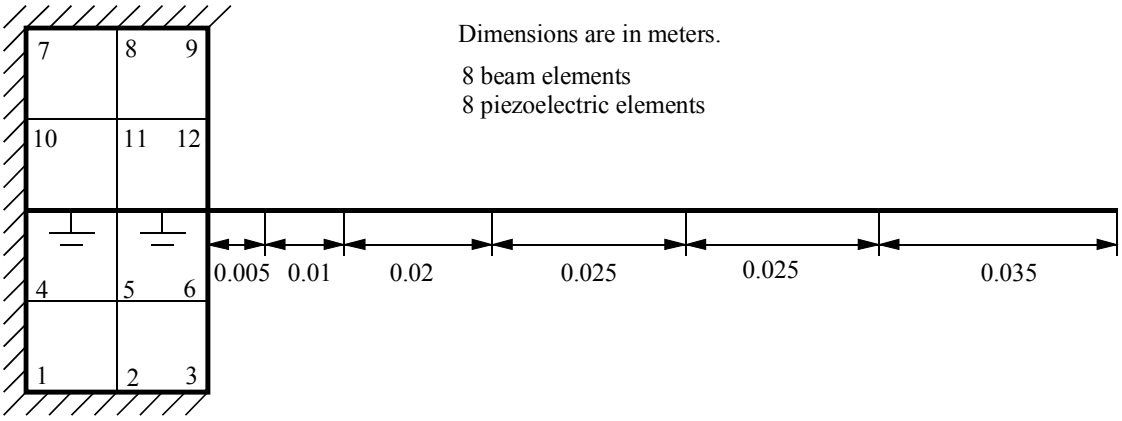

Figure 3.3 FE model for the beam and PZT's used for the validation.

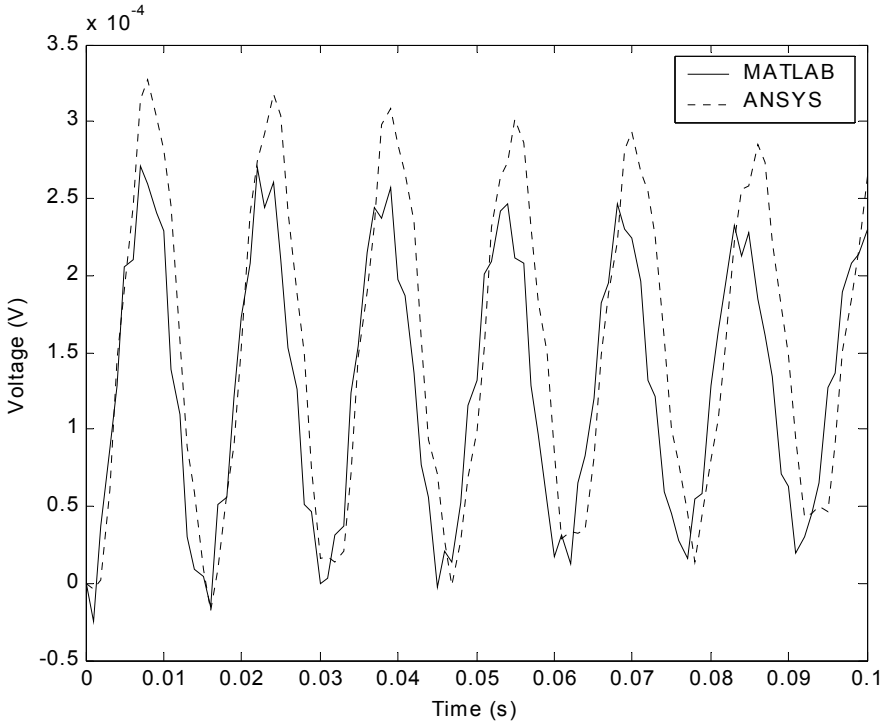

Figure 3.4 Voltage outputs at node 7 for a unit step input.

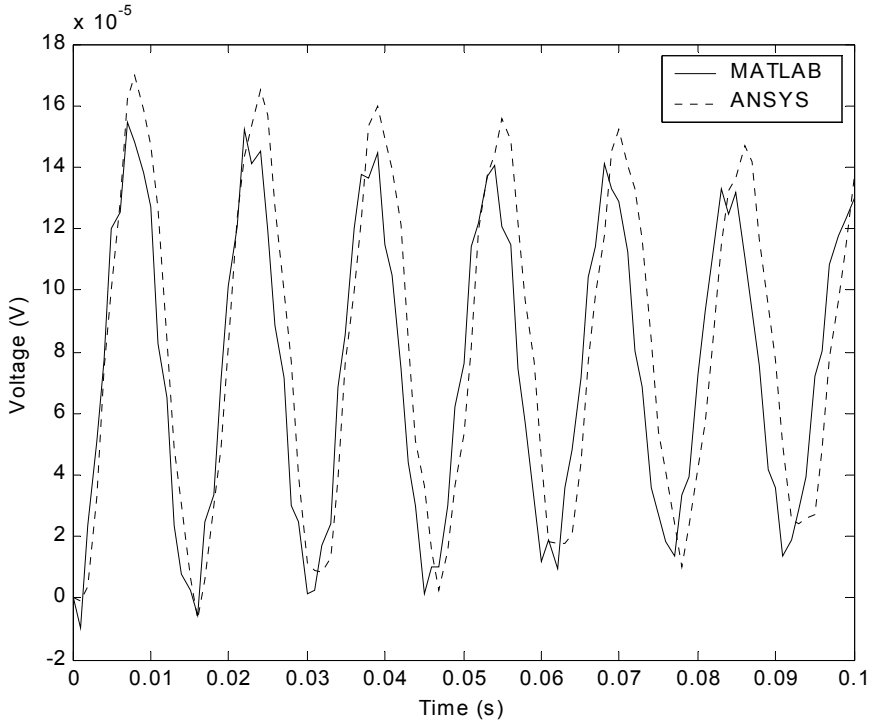

Figure 3.5 Voltage outputs at node 9 for a unit step input.

TABLE 3.2 First three natural frequencies in Hz. (beam with PZT's)

	MATLAB	ANSYS
1	65.49	65.53
2	410.77	410.96
3	1153.0	1153.3

Before we start our study, we have to check that our actuator locations do not interface with the modal nodes. That is, the actuator node where we feed the input voltages should not be on the same location of the modal nodes, i.e. transverse displacement should not be zero.

Figures 3.6 – 3.8, show the first three mode shapes for the beam with the PZT actuator placed 5 mm from the fixed end. Table 3.3 gives the values for the transverse displacement at node 5 (see Figure 3.2) for the first three mode shapes at each PZT actuator location.

As we can see from Table 3.3, in all the cases, node 5 has values for the transverse displacement other than zero. So we can conclude from the table that the actuator can be placed in all those locations. Moreover, with the controller included, the vibrations can be controlled at those locations.

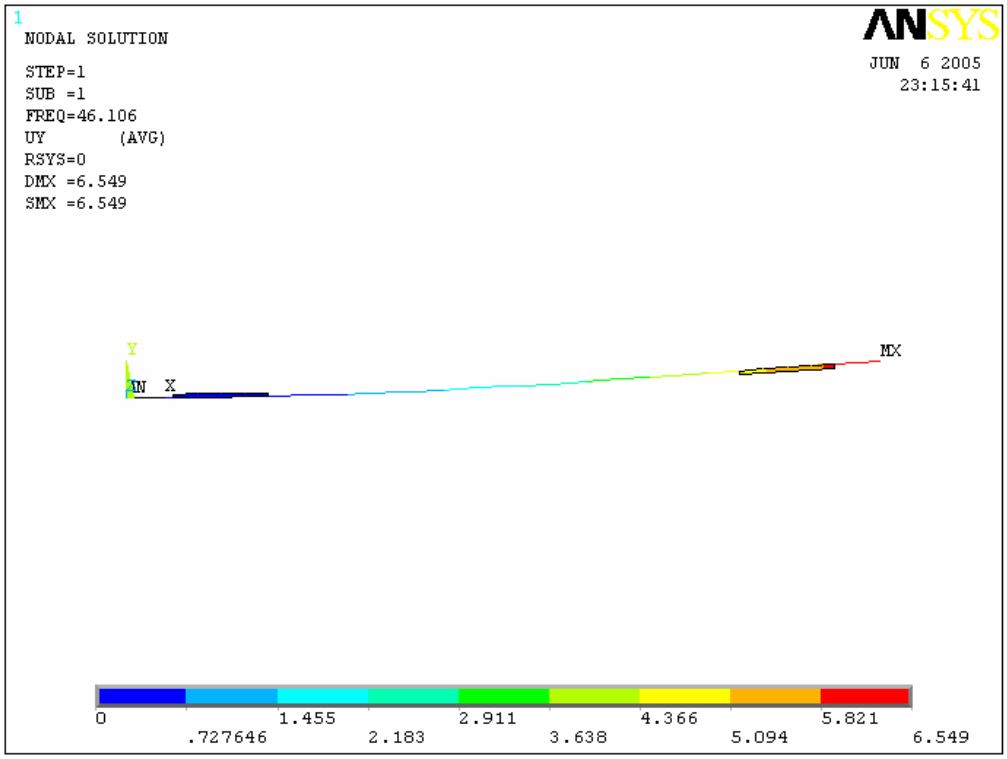

Figure 3.6 1st mode shape for the beam with PZT's (PZT actuator placed 5 mm from the fixed end).

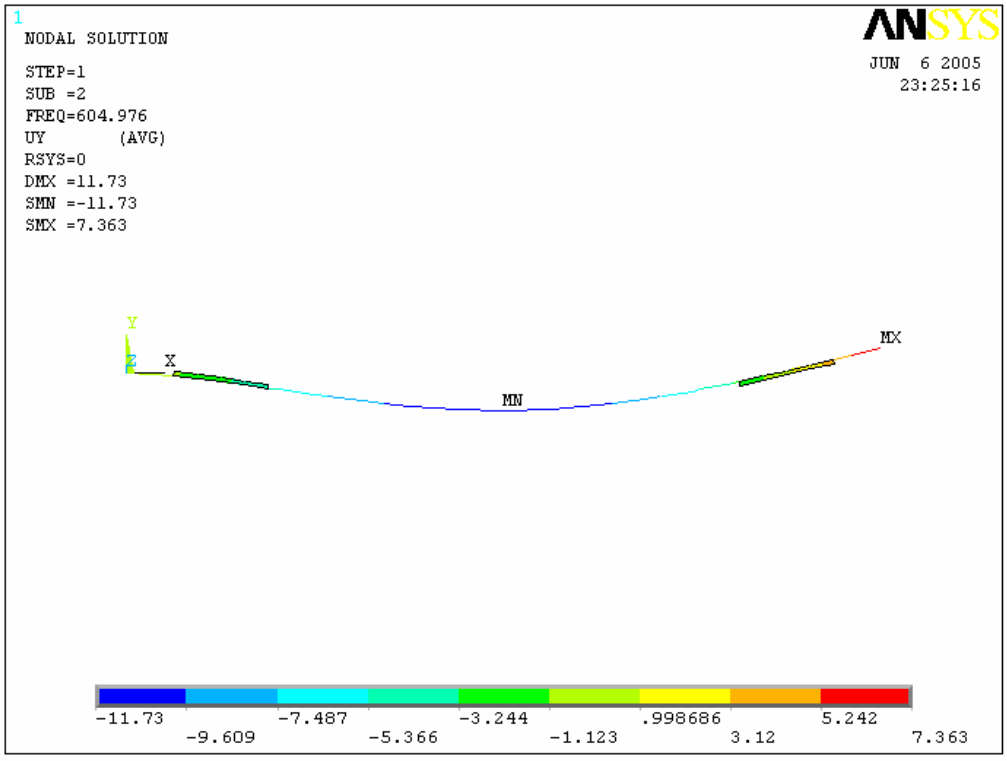

Figure 3.7 2nd mode shape for the beam with PZT's (PZT actuator placed 5 mm from the fixed end).

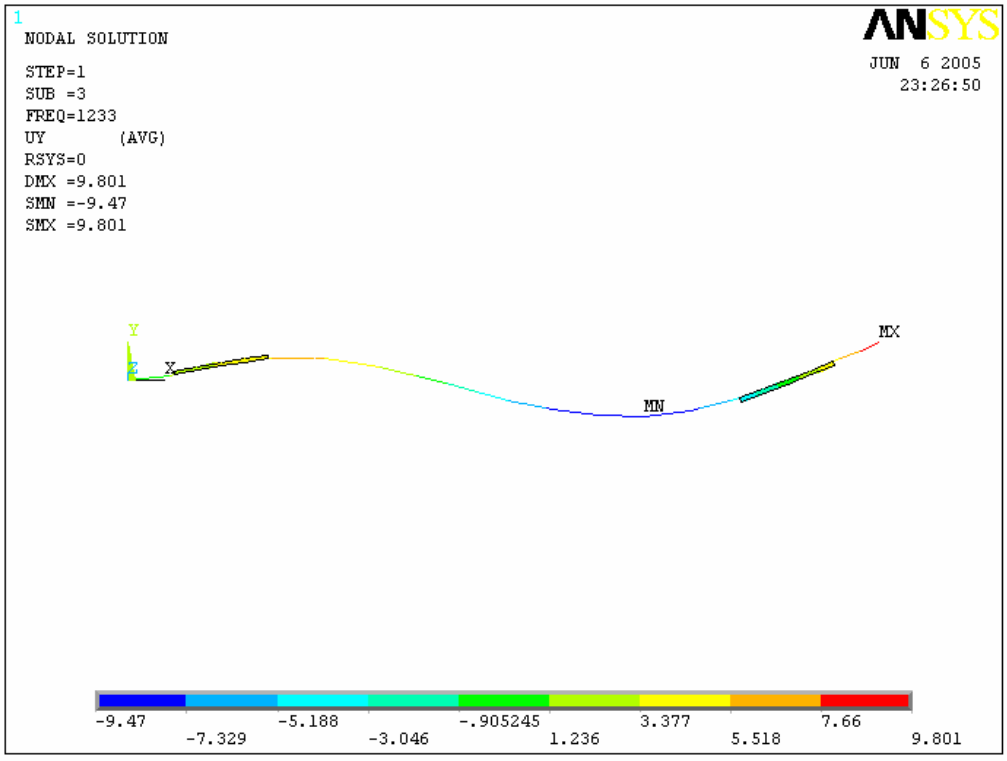

Figure 3.8 3rd mode shape for the beam with PZT's (PZT actuator placed 5 mm from the fixed end).

TABLE 3.3 Transverse displacements for node 5 of the actuator for the first three mode shapes of the beam with PZT's.

Location (from fixed end)	**Mode Shape**	**Frequency (Hz)**	**Displacement**
5 mm	1st mode	46.016	0.32141
5 mm	2nd mode	604.976	-4.9201
5 mm	3rd mode	1233	5.5120
15 mm	1st mode	44.336	0.95776
15 mm	2nd mode	385.521	-6.0748
15 mm	3rd mode	1197	1.3826
20 mm	1st mode	132.41	3.7923
20 mm	2nd mode	411.98	-4.3188
20 mm	3rd mode	1394	-3.1248
25 mm	1st mode	42.301	1.7350
25 mm	2nd mode	304.152	-5.5271
25 mm	3rd mode	1362	-1.4421
35 mm	1st mode	39.748	2.5323
35 mm	2nd mode	292.527	-4.6329
35 mm	3rd mode	1545	-3.8977
40 mm	1st mode	81.230	5.5361
40 mm	2nd mode	534.62	0.020373
40 mm	3rd mode	1165.8	-2.4540
45 mm	1st mode	36.742	3.2465
45 mm	2nd mode	338.405	-3.2314
45 mm	3rd mode	1663	-4.6054
60 mm	1st mode	51.094	5.9164
60 mm	2nd mode	638.85	3.7533
60 mm	3rd mode	1270.7	4.3590

3.3 CASE 1: LQR CONTROLLER

In this case, an LQR controller is added to the system. The output voltages at node 10 of the sensor will be fed to the LQR controller then to node 5 of the actuator (Figure 3.9).

The actuator will be placed in five different positions, which are at 0.005, 0.015, 0.025, 0.035 and 0.045 m from the fixed end. The sensor location, as we mentioned earlier, will be fixed throughout the simulations to ensure that we have the same output voltages fed to the actuator.

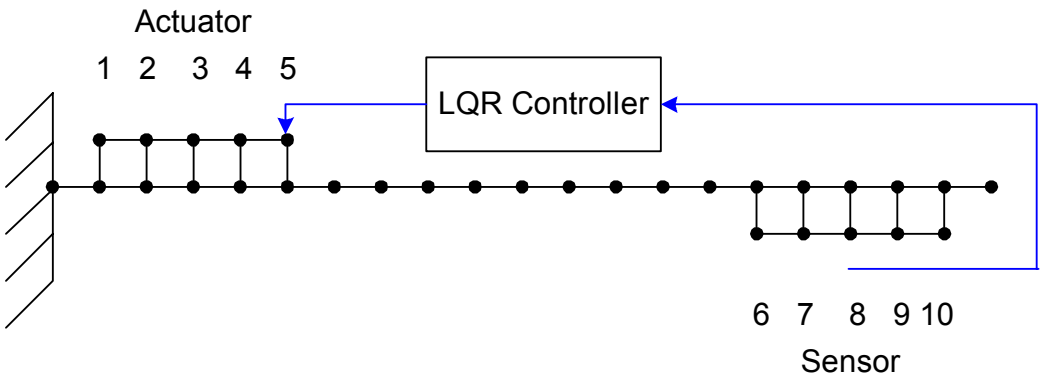

Figure 3.9 Beam-PZT's system with LQR controller.

For the system with the LQR controller, the closed-loop state equation is written as follows:

$$\dot{z} = (A - BK)z + B_f f \tag{3.12}$$

Where K is the optimum gain matrix determined as follows:

We want to minimize the performance index defined as:

$$J = \int_0^\infty \left(x^T Q x + u^T R u \right) dt \tag{3.13}$$

Where Q and R are the state and input weight matrices respectively.

So to minimize the performance index, we obtain the feedback as:

$$u = -Kx \tag{3.14}$$

Where K is the optimal gain matrix obtained as:

$$K = B^T S_c \tag{3.15}$$

and S_c is the solution of the controller algebraic Riccati equation

$$A^T S_c + S_c A - S_c B B^T S_c + Q = 0 \tag{3.16}$$

The closed-loop eigenvalues of the system, i.e. the eigenvalues of the close-loop state matrix (*A-BK*) in Eq. (3.12), are computed and shown in Figure 3.10. The damping matrix C_{uu} is taken as zero matrix in numerical computations. As we can

see, all the eigenvalues lie in the left hand side, which means that the closed-loop system is stable.

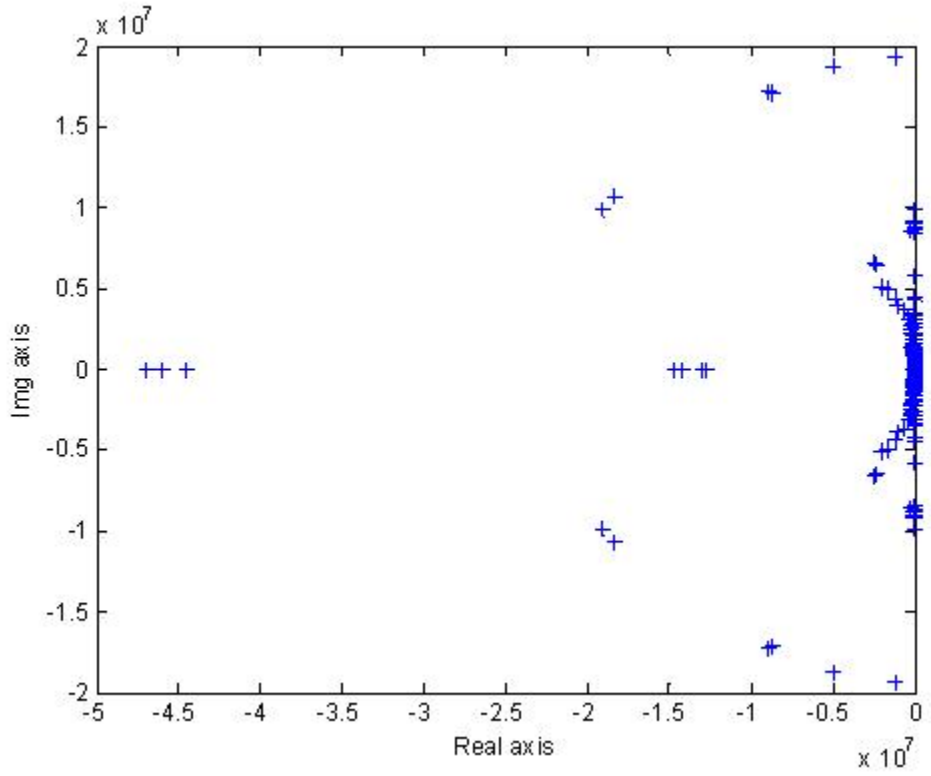

Figure 3.10 Closed-loop eigenvalues for the beam and PZT's with LQR controller.

The closed-loop sensor voltages from node 10 of the PZT sensor for the five different locations of the PZT actuator are shown in the results. The weighting matrices for the LQR, Q and R, are 10^{-7} x I (2 * ndof) and I (nvolt) respectively. Where ndof and nvolt are number of mechanical degrees of freedom and number of volt degrees of freedom respectively, and I is the identity matrix with the size given between the brackets.

3.4 CASE 2: LQG CONTROLLER

This case is similar to case 1 except that a different control technique will be used. An LQG controller will be used for the same system of beam and PZT actuator and sensor. The output voltages from node 10 of the sensor will be fed to node 5 of the actuator.

Since the LQG performs better than the LQR, so the effect of the actuator placement might not be clear for the PZT's arrangement used in case1. Figure 3.11 shows the arrangement that will be used for this case. The FE mesh will be same as case1. The system with the LQG controller is shown in Figure 3.12.

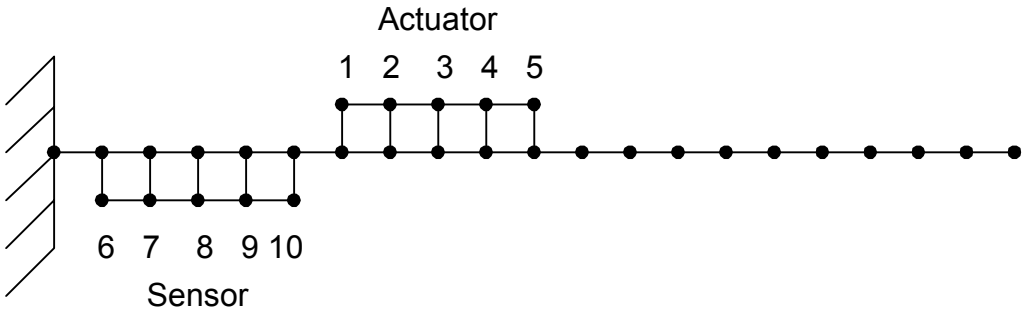

Figure 3.11 Finite element mesh of the beam & PZT's system (2).

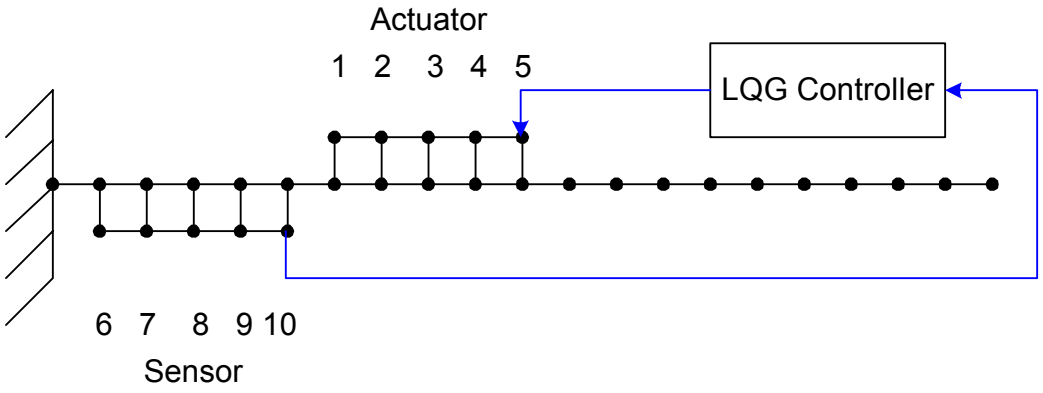

Figure 3.12 Beam-PZT's system with LQG controller.

In this case, the actuator will be placed in three different locations. These locations are 0.02, 0.04 and 0.06 m from the fixed end of the beam. The closed-loop eigenvalues for the system with the LQG controller are shown in Figure 3.13.

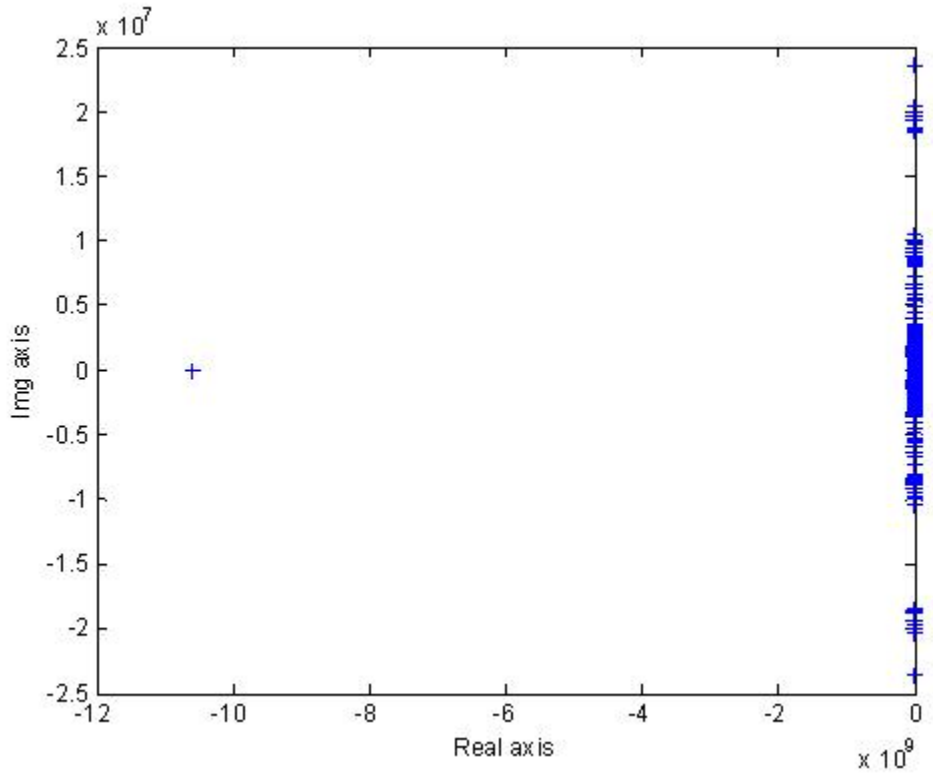

Figure 3.13 Closed-loop eigenvalues for the beam and PZT's with LQG controller.

The damping matrix C_{uu} is taken as zero matrix in numerical computations. The sensor voltages from node 10 of the PZT sensor for the three locations of the PZT actuator are shown in the results. The weighting matrices for the LQR part of the LQG controller, Q and R, are taken as follows: 0.005 x I (2 x ndof) and 1. The weighting matrices for the Kalman estimator, Qe and Re, are taken as 5 x 10^6 x I (2) and 10^{-5}.

3.5 RESULTS and DISCUSSION

3.5.1 CASE 1: LQR CONTROLLER

To compare the open loop and the closed loop system with the LQR controller included, Figure 3.14 shows the Bode diagram for both systems. It is clear that there is small phase change for the closed-loop system compared with the open-loop system. For the magnitude, the closed-loop system has higher values at certain frequencies, but as the frequency increase, the magnitude becomes less than the open-loop system.

Figures 3.15 – 3.19, show the sensor voltages outputs for the five different locations of the actuator. The output voltages are measured from node 10 of the sensor.

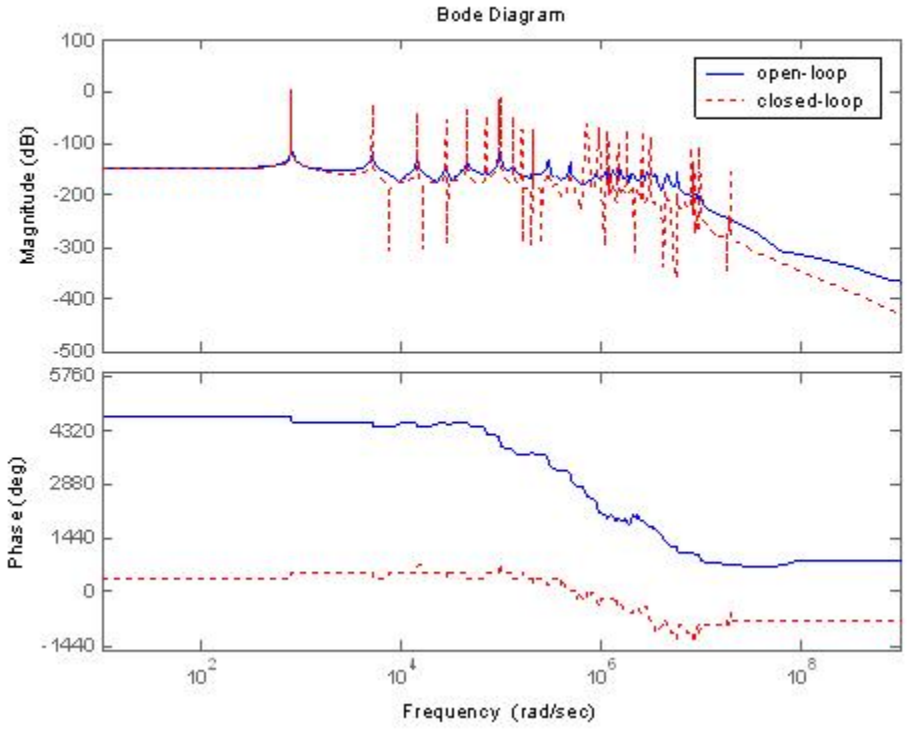

Figure 3.14 Bode diagram for the closed-loop and the open-loop systems for the beam-PZT's with LQR controller.

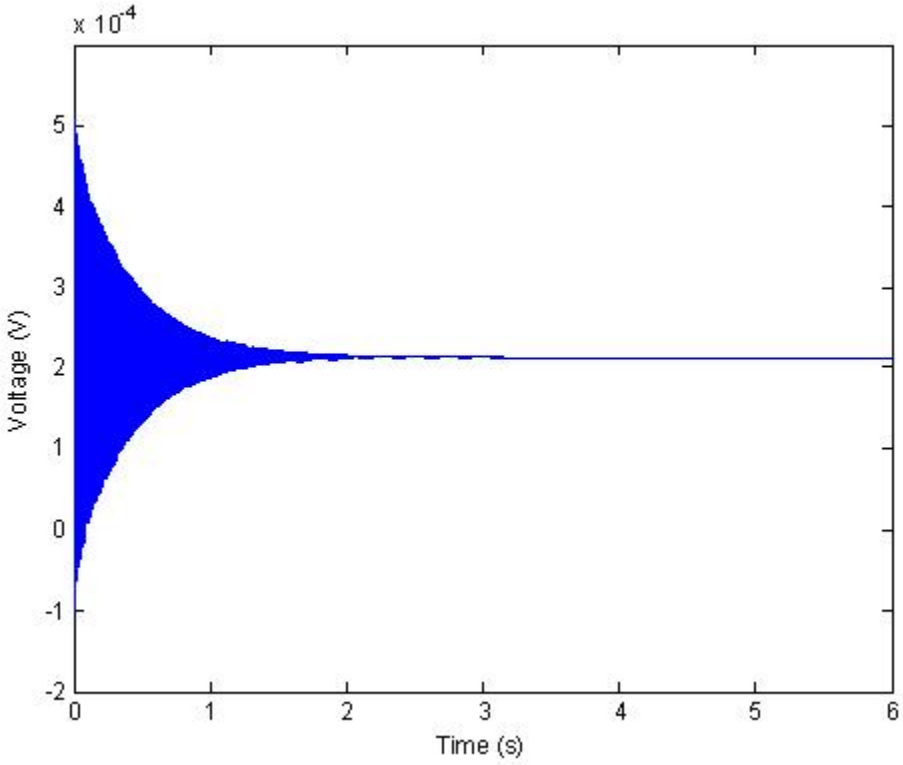

Figure 3.15 Closed-loop sensor voltages (PZT actuator placed 0.005 m from the fixed end of the beam) with an LQR controller.

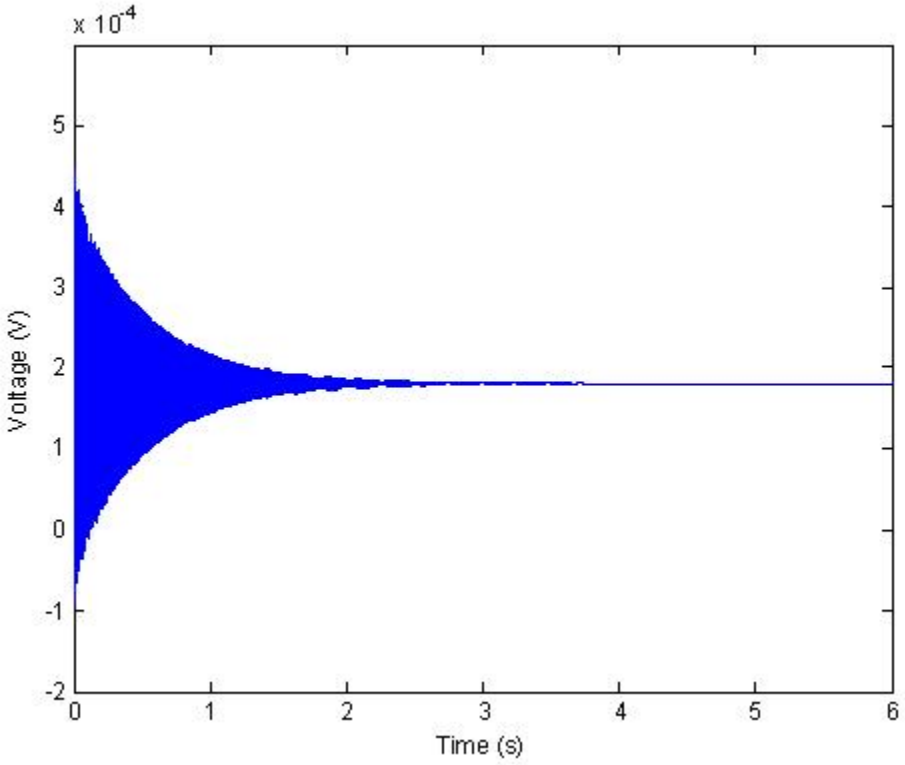

Figure 3.16 Closed-loop sensor voltages (PZT actuator placed 0.015 m from the fixed end of the beam) with an LQR controller.

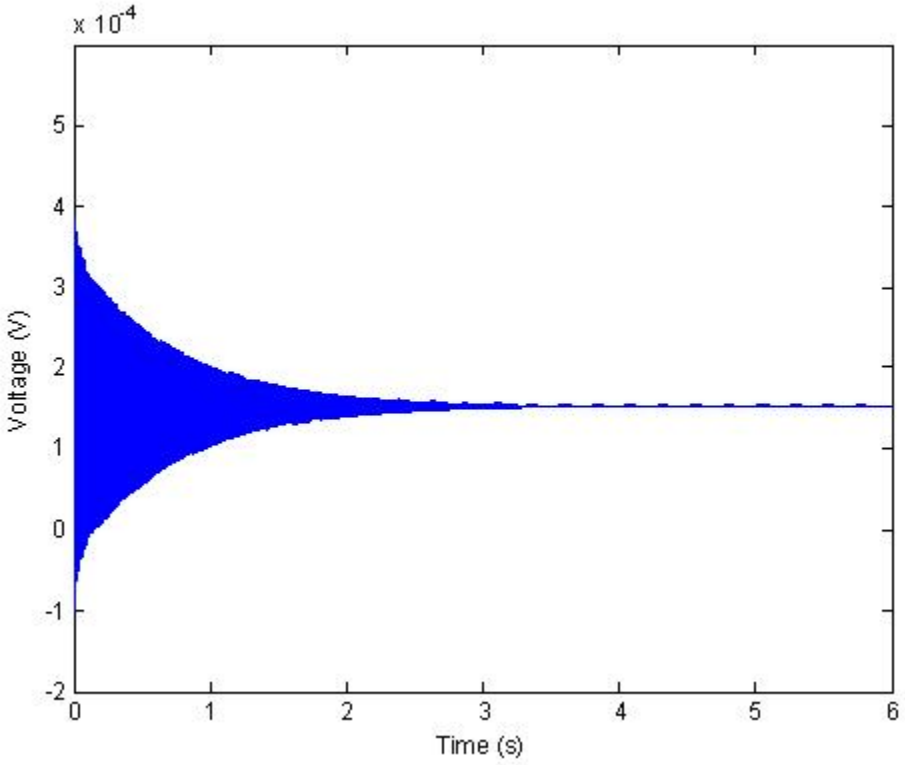

Figure 3.17 Closed-loop sensor voltages (PZT actuator placed 0.025 m from the fixed end of the beam) with an LQR controller.

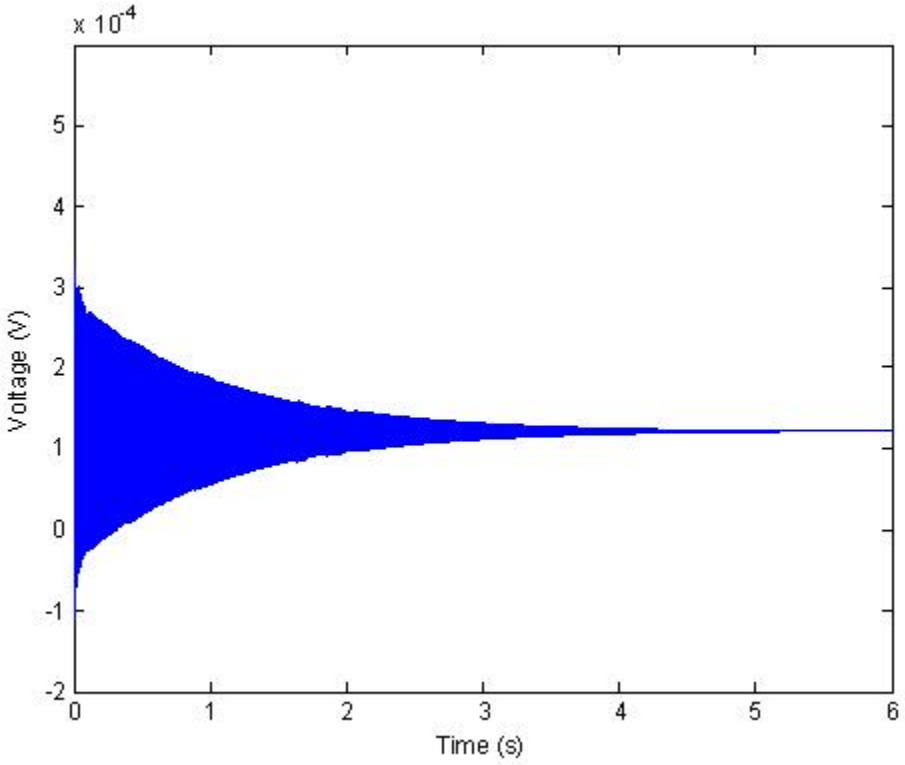

Figure 3.18 Closed-loop sensor voltages (PZT actuator placed 0.035 m from the fixed end of the beam) with an LQR controller.

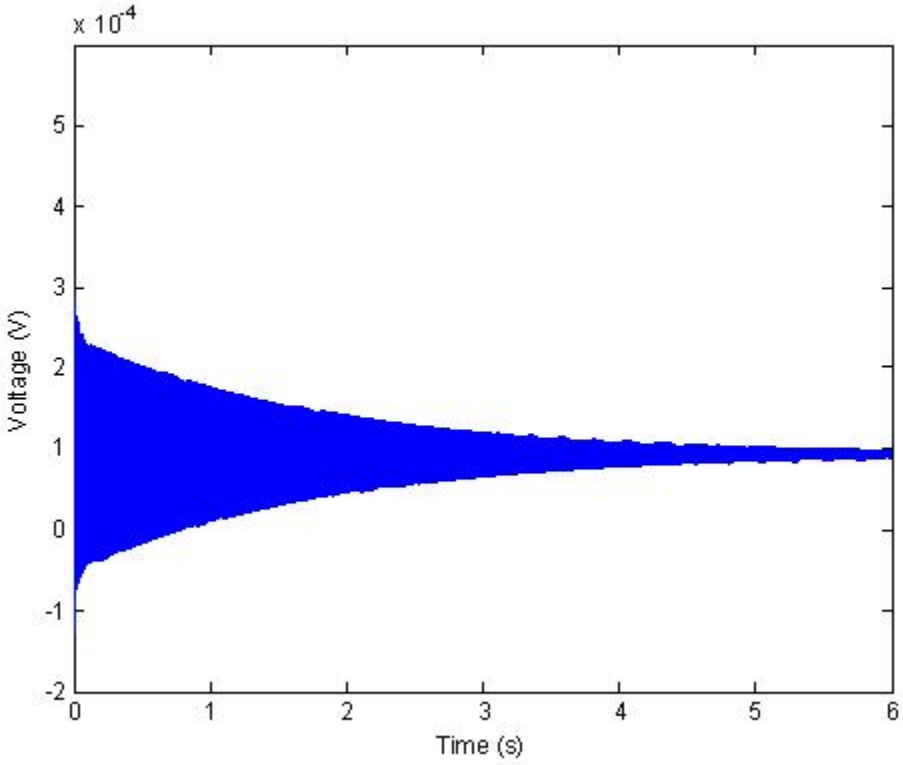

Figure 3.19 Closed-loop sensor voltages (PZT actuator placed 0.045 m from the fixed end of the beam) with an LQR controller.

In terms of the settling time, placing the actuator closer to the fixed end of the beam performs better in attenuating structural vibrations of the system. Whereas, in terms of the vibration magnitude, placing the actuator far from the fixed end of the beam gives better results.

If we compare the two terms, we can see that the decrease rate in the settling time value is higher than the increase rate in the vibration magnitude as we place the actuator closer to the fixed end of the beam. The settling time for the first case, actuator placed 0.005 m from the fixed end, is approximately 3 sec, whereas the settling time for the last case, actuator placed 0.045 m from the fixed end, is more than 6 sec. Hence, it is better to place the actuator close to the beam support for better vibration management.

3.5.2 CASE 2: LQG CONTROLLER

The bode diagram is shown in Figure 3.20 for both open-loop and closed-loop systems for the beam-PZT's system with the LQG controller. As it is clear from the figure, the magnitude of the closed-loop system is less than the open-loop system. At the corner frequency, the magnitude of the closed-loop system gets high, but then it decreases as the frequency increases.

The phase angle change is small for both systems, but is has less change in the case of the closed-loop system. As it is clear in Figure 3.20, the phase angle for the closed-loop system is closer to zero than the open-loop system.

Figures 3.21 – 3.23, show the output voltages for the three different locations of the actuator. The output voltages are measured from node 10 of the sensor.

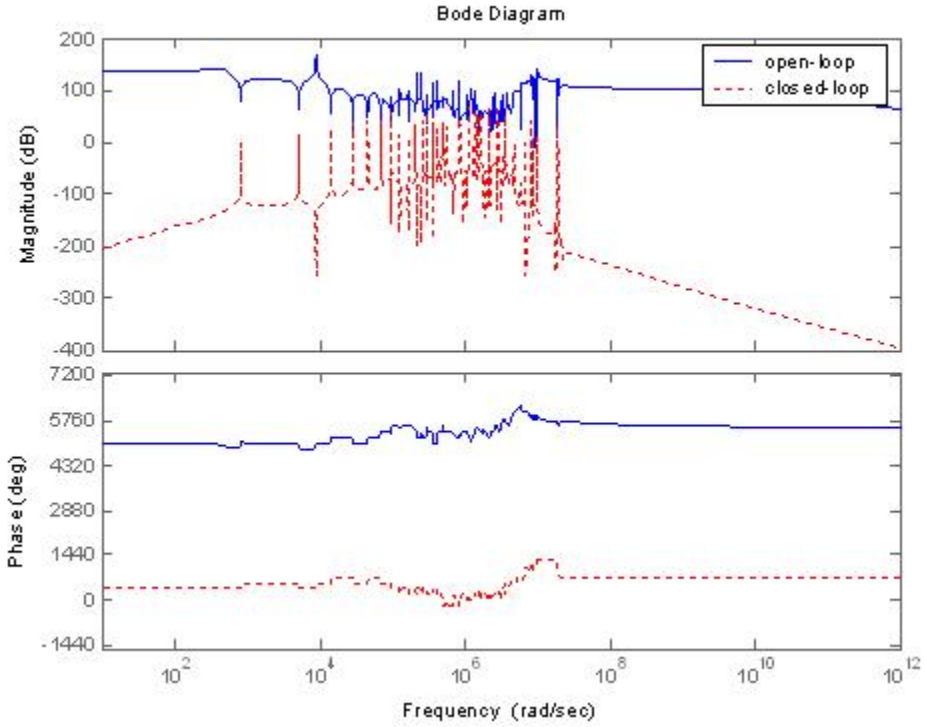

Figure 3.20 Bode diagram for the closed-loop and the open-loop systems for the beam-PZT's with LQG controller.

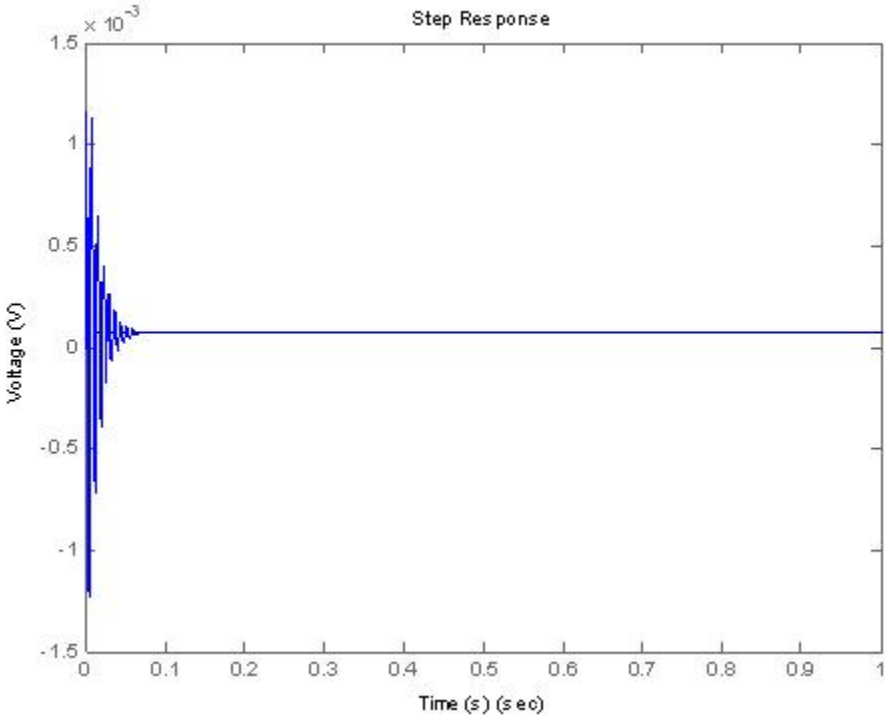

Figure 3.21 Closed-loop sensor voltages (PZT actuator placed 0.02 m from the fixed end of the beam) with an LQG controller.

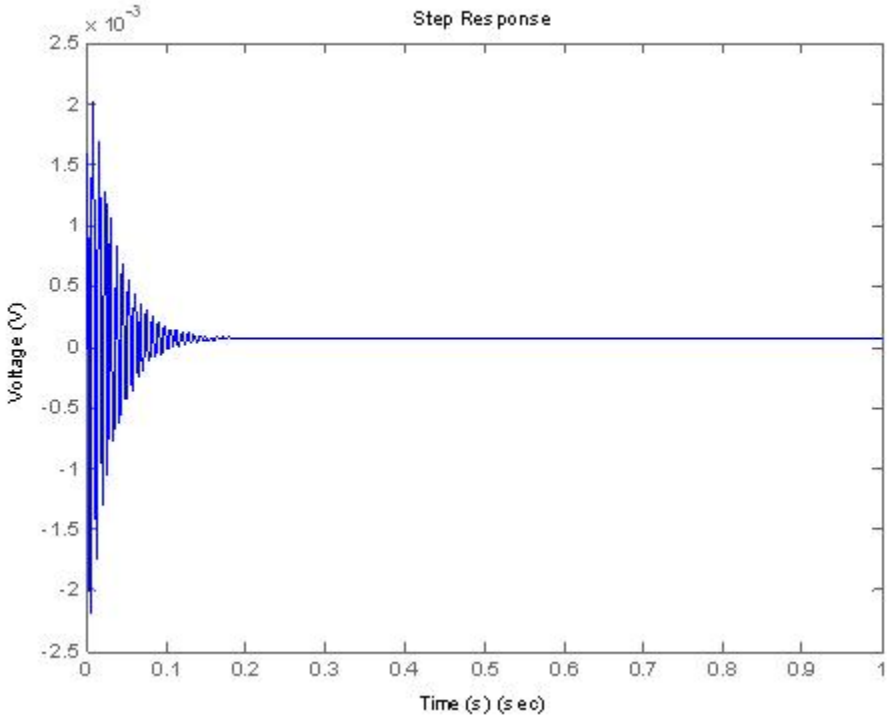

Figure 3.22 Closed-loop sensor voltages (PZT actuator placed 0.04 m from the fixed end of the beam) with an LQG controller.

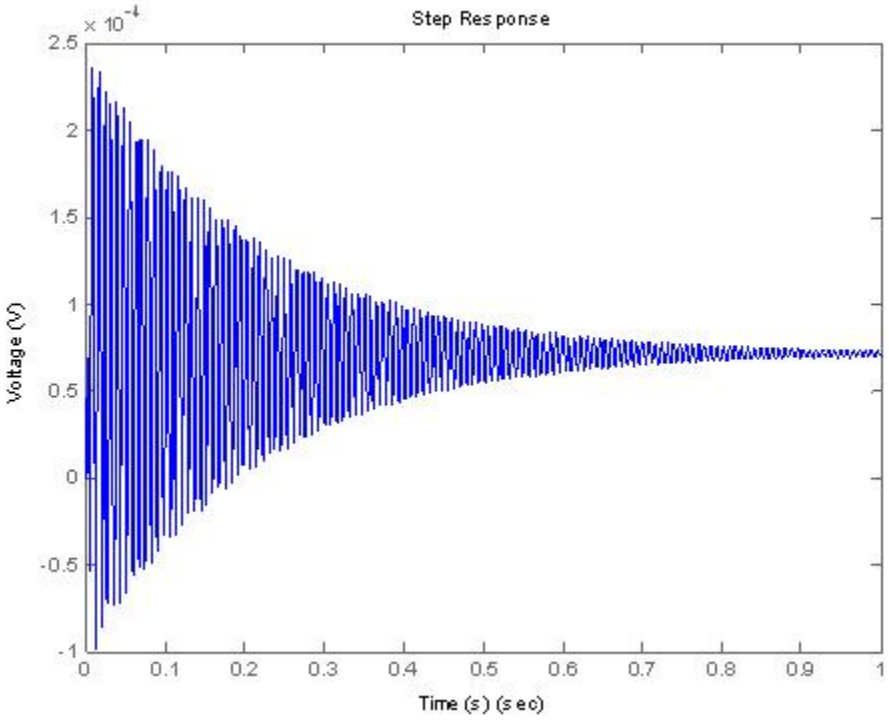

Figure 3.23 Closed-loop sensor voltages (PZT actuator placed 0.06 m from the fixed end of the beam) with an LQG controller.

As we can see, placing the PZT actuator closer to the fixed end of the beam gives better results in attenuating the structural vibrations. Also it is clear that as we place the PZT actuator far from the fixed end, the settling time increases in high rate.

At a distance of 0.02 m from the fixed end of the beam, the settling time was less than 0.1 sec, whereas at a distance of 0.04 m, the settling time was close to 0.2 sec. Then, at a distance of 0.06 m from the fixed end the settling time was more than 1 sec. So it is clear that as we move away from the fixed end, the increase rate for the settling time is increasing.

So we conclude from the two cases, that as we place the PZT actuator closer to the fixed end, we get better results in controlling the structural vibrations in terms of the settling time. One can notice the difference in the vibration magnitude between locations close to the fixed end, and locations far from the fixed end. The rate in which the vibration magnitude decreases as we move far from the fixed end, is less than the rate in which the settling time increases as we move far from the fixed end.

CHAPTER 4

PLATE WITH PZT ACTUATOR AND SENSOR

4.1 PROBLEM DEFINITION

In this chapter, a smart system consisting of a plate fixed at one side and mounted with a PZT sensor and a PZT actuator is tested for vibration control (Figure 4.1). The length, width and thickness of the plate are 0.1, 0.03 and 0.002 m, respectively. For the PZT sensor and actuator, the length, width and thickness are taken as 0.02, 0.01 and 0.002 m, respectively. The material properties are listed in Table 4.1.

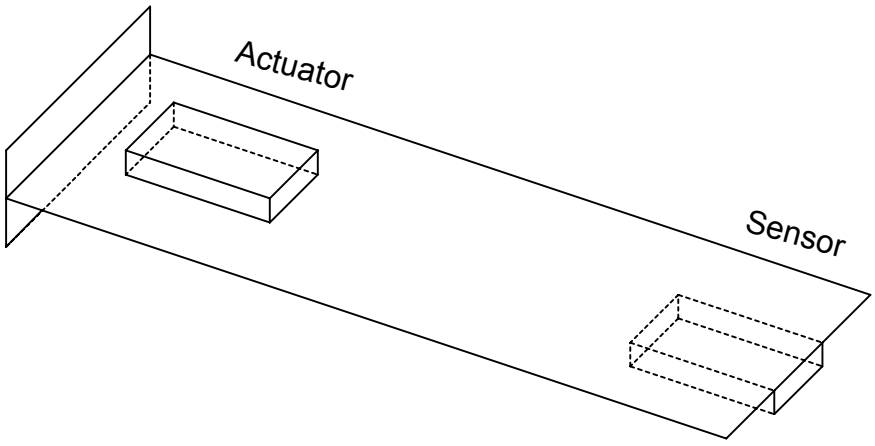

Figure 4.1 Smart system consisting of plate, PZT sensor and PZT actuator.

TABLE 4.1 Material Properties for the plate with PZT's

Piezoceramic (BM500) [13].	
c_{11} (Pa)	1.26×10^{11}
c_{12} (Pa)	8.41×10^{10}
c_{13} (Pa)	7.95×10^{10}
c_{22} (Pa)	1.17×10^{11}
c_{23} (Pa)	8.41×10^{10}
c_{33} (Pa)	1.26×10^{11}
c_{44} (Pa)	2.3×10^{10}
c_{55} (Pa)	2.3×10^{10}
c_{66} (Pa)	2.35×10^{10}
e_{12} (C/m^2)	-5.4
e_{22} (C/m^2)	15.8
e_{32} (C/m^2)	-5.4
e_{41} (C/m^2)	12.3
e_{53} (C/m^2)	12.3
ε_{11} (F/m)	1.151×10^{-3}
ε_{22} (F/m)	1.043×10^{-3}
ε_{33} (F/m)	1.151×10^{-3}
ρ (kg/m^3)	7800

Beam (St)	
Y (Pa)	2.07×10^{11}
ν	0.3
ρ (kg/m^3)	7800

In this chapter, a similar study to the one done in chapter 3 will be done for a plate structure. The location of the sensor will be fixed throughout the numerical simulations. The actuator location will be varied through six different locations, and the effect of the actuator placement on controlling the vibration of the plate will be studied.

Since for the plate case we work in 3-D, we can have more options when varying the location of the PZT actuator. For this case, plate with PZT's, the location of the actuator will be changed in both in-plane axes of the plate.

As in chapter 3, two types of control techniques will be used. The first will be done with an LQR controller and the second will be done with a LQG controller. A unit step force will be applied in the positive perpendicular direction at the tip of the plate.

4.2 MODELING

An FE model will be done in MATLAB for our system. The PZT actuator and sensor will be modeled using the linear piezoelectric equations discussed in chapter 2. The plate FE matrices and equations are derived next.

For our plate model we have five DOF, u, v, w, θ_x and θ_y. The modeling for the plate will be done in two parts, the first one will handle the in-plane motion, and the second one will handle the two rotational and the vertical displacement. Then at the end, when we model the plate in MATLAB, the stiffness and mass matrices will be added to each other.

Figure 4.2 shows the plate element with the in-plane nodal degrees of freedom.

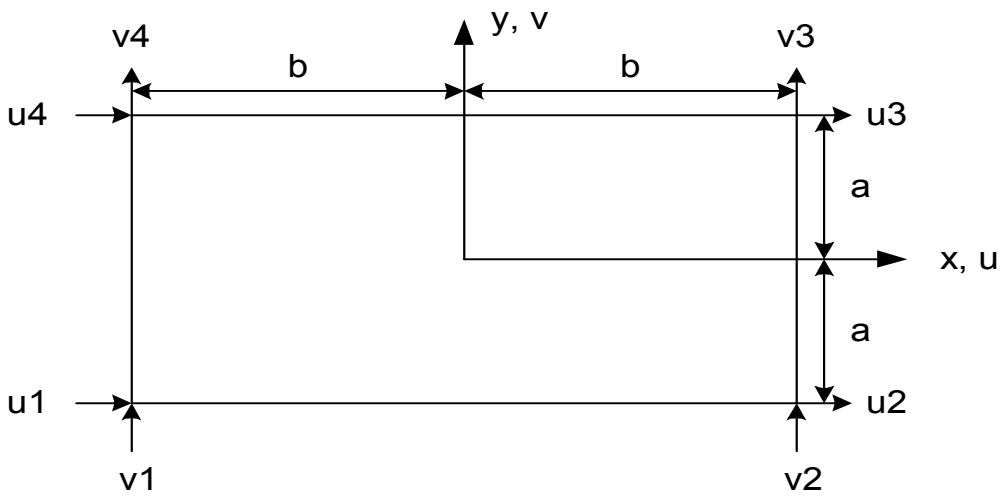

Figure 4.2 Basic 4-node plane stress rectangular element with nodal DOF.

A compatible displacement functions for the element shown in Figure 4.1 must be linear along the edges. The linear displacement functions are chosen as:

$$\begin{aligned} u(x,y) &= a_1 + a_2 x + a_3 y + a_4 xy \\ v(x,y) &= a_5 + a_6 x +_7 y + a_8 xy \end{aligned} \tag{4.1}$$

Then after substituting the boundaries values in Eq. (4.1), we obtain the following:

$$\begin{aligned} u(x,y) &= \frac{1}{4ab}[(b-x)(a-y)u_1 + (b+x)(a-y)u_2 \\ &\quad + (b+x)(a+y)u_3 + (b-x)(a+y)u_4] \\ v(x,y) &= \frac{1}{4ab}[(b-x)(a-y)v_1 + (b+x)(a-y)v_2 \\ &\quad + (b+x)(a+y)v_3 + (b-x)(a+y)v_4] \end{aligned} \tag{4.2}$$

Eq. (4.2) can be expressed in terms of the shape functions and unknown nodal displacements as:

$$\{\psi\} = [N]\{d\} \tag{4.3}$$

where the shape functions are as follows:

$$\begin{aligned} N_1 &= \frac{(b-x)(a-y)}{4ab} & N_2 &= \frac{(b+x)(a-y)}{4ab} \\ N_3 &= \frac{(b+x)(a+y)}{4ab} & N_4 &= \frac{(b-x)(a+y)}{4ab} \end{aligned} \tag{4.4}$$

Now we can write Eq. (4.3) in expended form:

$$\begin{Bmatrix} u \\ v \end{Bmatrix} = \begin{bmatrix} N_1 & 0 & N_2 & 0 & N_3 & 0 & N_4 & 0 \\ 0 & N_1 & 0 & N_2 & 0 & N_3 & 0 & N_4 \end{bmatrix} \begin{Bmatrix} u_1 \\ v_1 \\ \vdots \\ u_4 \\ v_4 \end{Bmatrix} \tag{4.5}$$

Now we will define the element strains for the 2-D dimensional stress state:

$$\begin{Bmatrix} \varepsilon_x \\ \varepsilon_y \\ \gamma_{xy} \end{Bmatrix} = \begin{Bmatrix} \dfrac{\partial u}{\partial x} \\ \dfrac{\partial v}{\partial y} \\ \dfrac{\partial u}{\partial y} + \dfrac{\partial v}{\partial x} \end{Bmatrix} \tag{4.6}$$

Using Eq. (4.5) in Eq. (4.6) and taking the derivatives of the displacements, we can write the strains in terms of the unknown nodal displacements as:

$$\{\varepsilon\} = [B]\{d\} \tag{4.7}$$

Before we define the mass and stiffness matrices, we will define the constitutive matrix for a plane stress as:

$$[D] = \frac{E}{1-\nu^2}\begin{bmatrix} 1 & \nu & 0 \\ \nu & 1 & 0 \\ 0 & 0 & \frac{1-\nu}{2} \end{bmatrix} \tag{4.8}$$

Now defining the elemental stiffness matrix in a similar way to beam elemental stiffness matrix, as follows:

$$[k] = \int_{-a}^{a}\int_{-b}^{b} [B]^T [D][B] t dx dy \tag{4.9}$$

where t is the thickness of the plate. The elemental mass matrix is defined also similar to the beam elemental mass matrix as:

$$[M] = \rho t \int_{-a}^{a}\int_{-b}^{b} [N]^T [N] dx dy \tag{4.10}$$

and the element force matrix is defined as:

$$\{f\} = \iiint_V [N]^T \{X\} dV + \{P\} + \iint_S [N_s]^T \{T\} dS \tag{4.11}$$

Now, after deriving the equations and matrices for the first part, we will derive the matrices for the second one. Figure 4.3 shows the plate element with the two rotational and the vertical DOF.

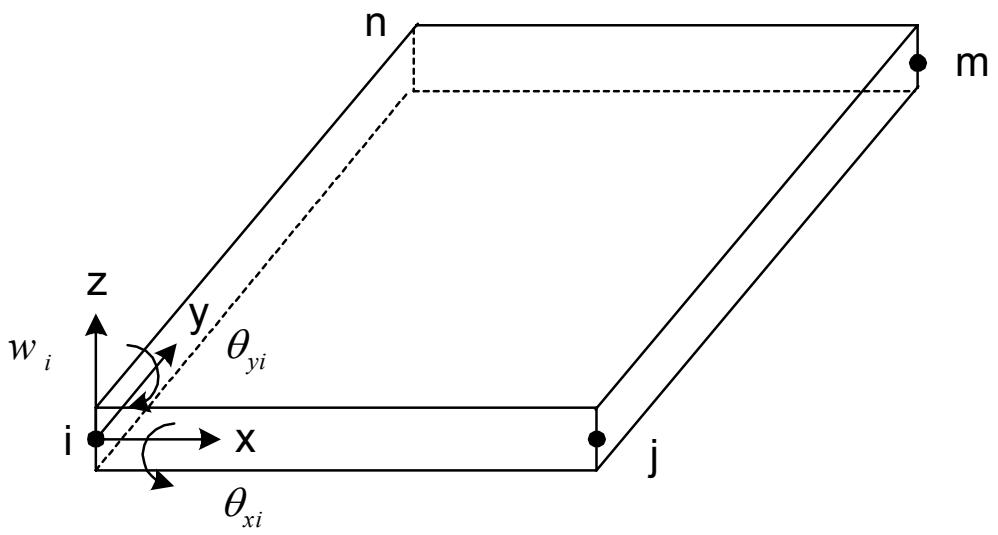

Figure 4.3 Rectangular plate element with nodal DOF.

As shown in Figure 4.3, we have 3 DOF per node for the plate element so we will select a 12-term polynomial in x and y as follows:

$$\begin{aligned} w = {} & a_1 + a_2 x + a_3 y + a_4 x^2 + a_5 xy + a_6 y^2 + a_7 x^3 \\ & a_8 x^2 y + a_9 x y^2 + a_{10} y^3 + a_{11} x^3 y + a_{12} x y^3 \end{aligned} \tag{4.12}$$

The constants in Eq. (4.12) can be determined by expressing the 12 equations linking the values of *w* and its slopes at the nodes. First we write

$$\begin{Bmatrix} w \\ +\dfrac{\partial w}{\partial y} \\ -\dfrac{\partial w}{\partial x} \end{Bmatrix} = \begin{bmatrix} 1 & x & y & x^2 & xy & y^2 & x^3 & x^2 y & x y^2 & y^3 & x^3 y & x y^3 \\ 0 & 0 & 1 & 0 & x & 2y & 0 & x^2 & 2xy & 3y^2 & x^3 & 3xy^2 \\ 0 & -1 & 0 & -2x & -y & 0 & -3x^2 & -2xy & -y^2 & 0 & -3x^2 y & -y^3 \end{bmatrix} \begin{Bmatrix} a_1 \\ a_2 \\ a_3 \\ \vdots \\ a_{12} \end{Bmatrix} \tag{4.13}$$

or in a simple matrix form

$$\{\psi\} = [P]\{a\} \tag{4.14}$$

Now, we evaluate Eq. (4.13) at each node as follows:

$$\begin{Bmatrix} w_i \\ \theta_{xi} \\ \theta_{yi} \\ w_j \\ \vdots \end{Bmatrix} = \begin{bmatrix} 1 & x_i & y_i & x_i^2 & x_i y_i & y_i^2 & x_i^3 & x_i^2 y_i & x_i y_i^2 & y_i^3 & x_i^3 y_i & x_i y_i^3 \\ 0 & 0 & 1 & 0 & x_i & 2y_i & 0 & x_i^2 & 2x_i y_i & 3y_i^2 & x_i^3 & 3x_i y_i^2 \\ 0 & -1 & 0 & -2x_i & -y_i & 0 & -3x_i^2 & -2x_i y_i & -y_i^2 & 0 & -3x_i^2 y_i & -y_i^3 \\ \vdots & & & & & & & & & & & \\ \cdots & & & & & & & & & & & \end{bmatrix} \begin{Bmatrix} a_1 \\ a_2 \\ \vdots \\ a_{12} \end{Bmatrix} \tag{4.15}$$

In compact form, Eq. (4.15) can be written as:

$$\{d\} = [C]\{a\} \tag{4.16}$$

From Eq. (4.16) the constants can be solved as follows:

$$[a] = [C]^{-1}\{d\} \tag{4.17}$$

Now, we can re-write Eq. (4.14) as:

$$\{\psi\} = [P][C]^{-1}\{d\} \tag{4.18}$$

or $$\{\psi\} = [N]\{d\} \tag{4.19}$$

where $[N] = [P][C]^{-1}$ is the shape function matrix.

Now we will define the curvature matrix by the rate of change of the angular displacements as:

$$\kappa_x = -\frac{\partial^2 w}{\partial x^2} \qquad \kappa_y = -\frac{\partial^2 w}{\partial y^2} \qquad \kappa_{xy} = -\frac{2\partial^2 w}{\partial x\,\partial y} \tag{4.20}$$

which gives us:

$$\begin{Bmatrix} \kappa_x \\ \kappa_y \\ \kappa_{xy} \end{Bmatrix} = \begin{Bmatrix} -2a_4 - 6a_7 - 2a_8 y - 6a_{11} xy \\ -2a_6 - 2a_9 x - 6a_{10} y + 6a_{12} xy \\ -2a_5 - 4a_8 - 4a_9 y - 6a_{11} x^2 - 6a_{12} y^2 \end{Bmatrix} \tag{4.21}$$

Expressing Eq. (4.21) in a matrix form gives:

$$\{\kappa\} = [Q]\{a\} \tag{4.22}$$

using Eq.(4.17) in Eq. (4.22) gives us:

$$\{\kappa\} = [B]\{d\} \tag{4.23}$$

where $[B] = [Q][C]^{-1}$ is the gradient matrix.

The constitutive matrix is defined as:

$$[D] = \frac{Et^3}{12(1-\nu^2)} \begin{bmatrix} 1 & \nu & 0 \\ \nu & 1 & 0 \\ 0 & 0 & \frac{1-\nu}{2} \end{bmatrix} \tag{4.24}$$

Now we can define the elemental matrices similar to the beam matrices. The stiffness, mass and force matrices can be found as in Eq.'s (4.9 - 4.11).

Using the derived equations and matrices, an FE program is written in MATLAB. The plate is meshed into 30 elements, and the PZT's are meshed into 2 elements each. Figure 4.4 shows the FE model for the plate and the PZT's. Plate and PZT's are meshed by with a line spacing of 0.01 m in each direction.

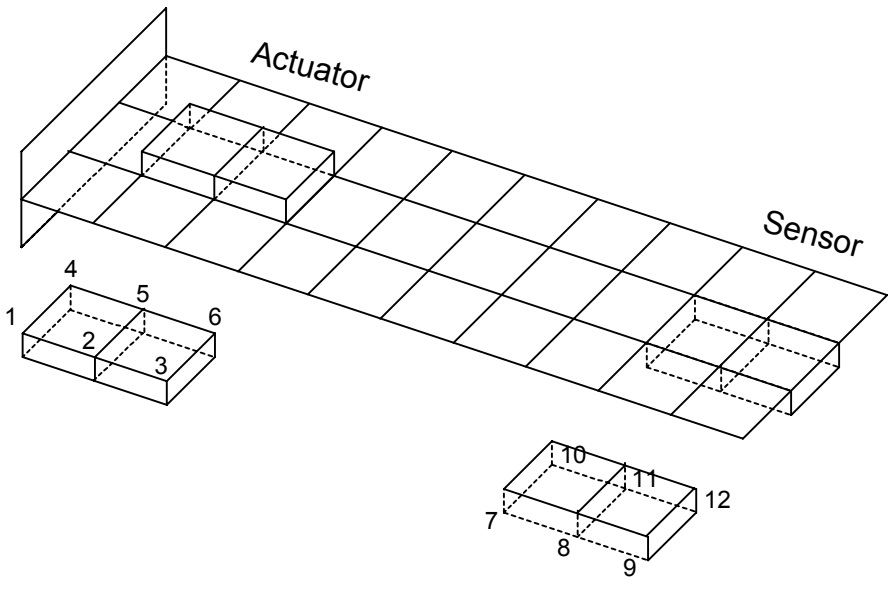

Figure 4.4 Finite element mesh of the plate & PZT's system.

Since we have five mechanical DOF for each node of the plate, the total mechanical DOF of the plate will be 236 (the nodes at the fixed side have zero DOF). Having the PZT's grounded at the boundary with the plate gives a total of 12 electrical DOF.

As we did in chapter 3, we will first compare our MATLAB model with ANSYS to check the reliability of our model. In ANSYS, the plate is modeled using an elastic 4-noded element (SHELL63) and the PZT's are modeled using a 3-D coupled element (SOLID5). Material properties are taken as in Table 4.1.

In both models, MATLAB and ANSYS, two unity static forces are applied at the tip of the plate. Figure 4.5 shows the FE model for the plate and PZT's as modeled in ANSYS.

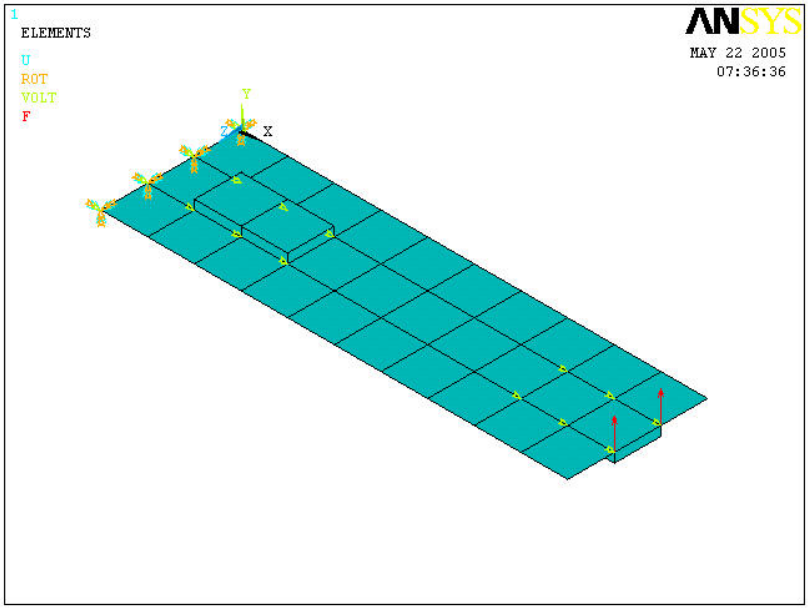

Figure 4.5 FE model for the plate and PZT's in ANSYS.

After applying the two unit static forces, the voltages will be compared for all the nodes of the sensor. Figure 4.6 shows the voltage reading for both PZT's nodes, i.e. nodes 1 – 12, for both MATLAB and ANSYS.

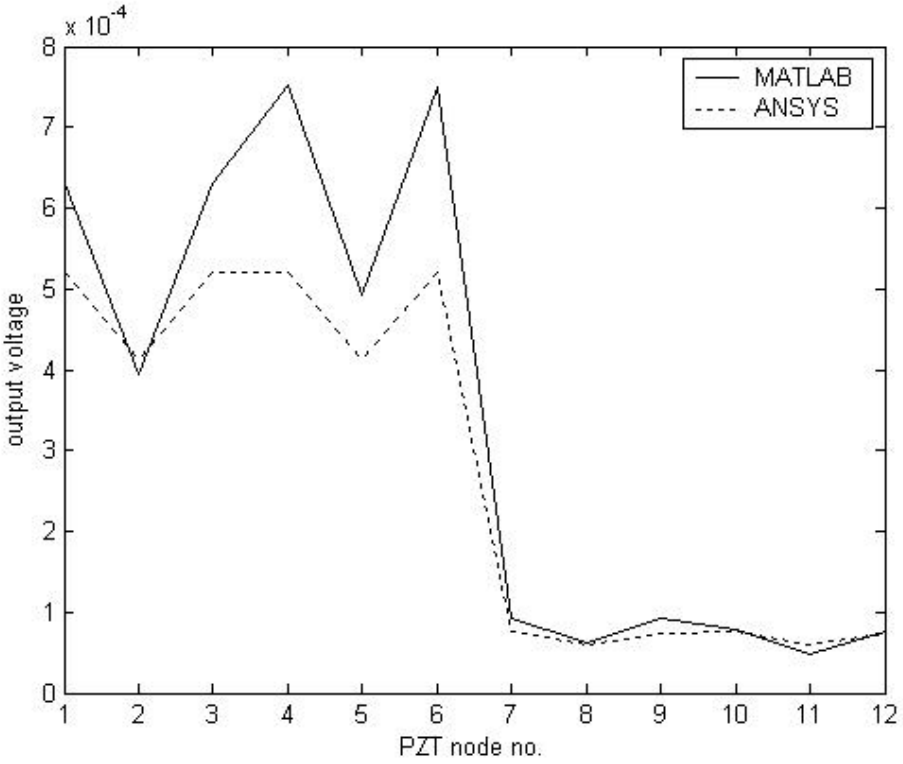

Figure 4.6 Voltage output for nodes 1 – 12 for a unit static force.

It is clear from Figure 4.6 that the behavior of the voltage output is quit similar between ANSYS and MATLAB. The values for the voltage output are almost the same, especially for the sensor nodes, which are more important for us since we read the output from them.

For both controllers that we will use in this chapter, the actuator will be placed in six different positions as shown in Figure 4.7. Note that each square is 0.01 x 0.01 m in size.

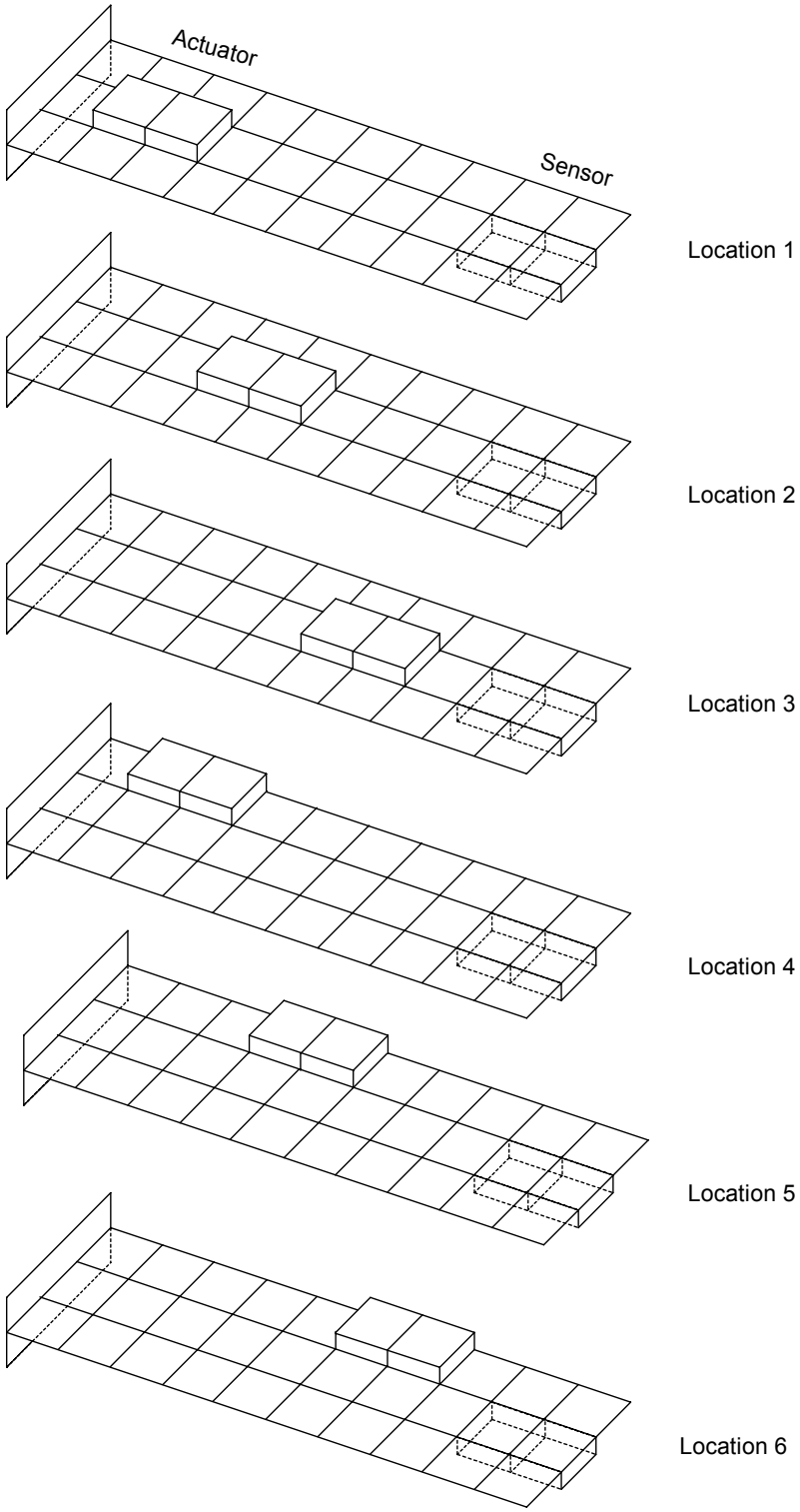

Figure 4.7 PZT actuator placements for numerical simulations.

After validating the FE model between MATLAB and ANSYS, we have to check the modal nodes. Since we are feeding the input voltages to actuator nodes 3 and 6, we have to make sure that these FE nodes are not modal nodes.

To check the modal nodes, we have to check the values for the transverse displacements for nodes 3 and 6 at each location and for the mode shapes. In our check we will go up to the 7^{th} mode shape.

Figures 4.8 – 4.14 show the first seven mode shapes for the plate with the PZT's for the first actuator location, that is location 1. Tables 4.2 – 4.7 shows the values for the transverse displacements for the actuator nodes 3 and 6 at each location for the first seven natural frequencies.

It is clear from Tables 4.2 – 4.7 that all the values for the transverse displacement are not zero. So from this step we can start the case study with controllers included for all the six locations (Figure 4.7).

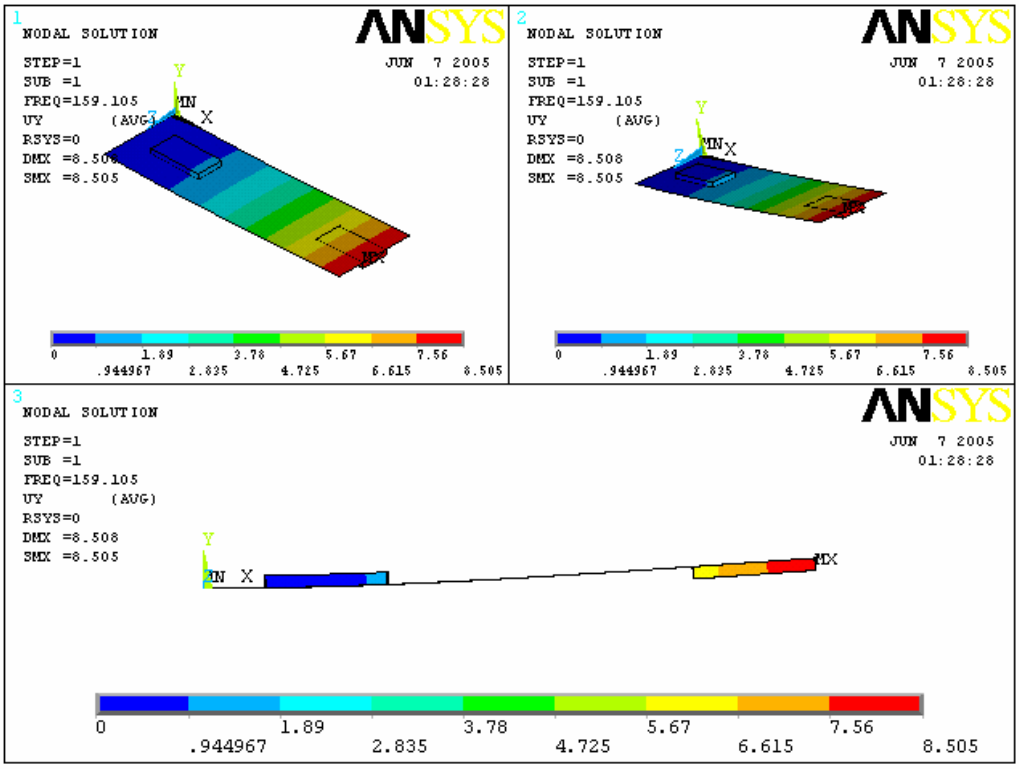

Figure 4.8 1st mode shape for the plate with PZT's
(PZT actuator placed at location 1).

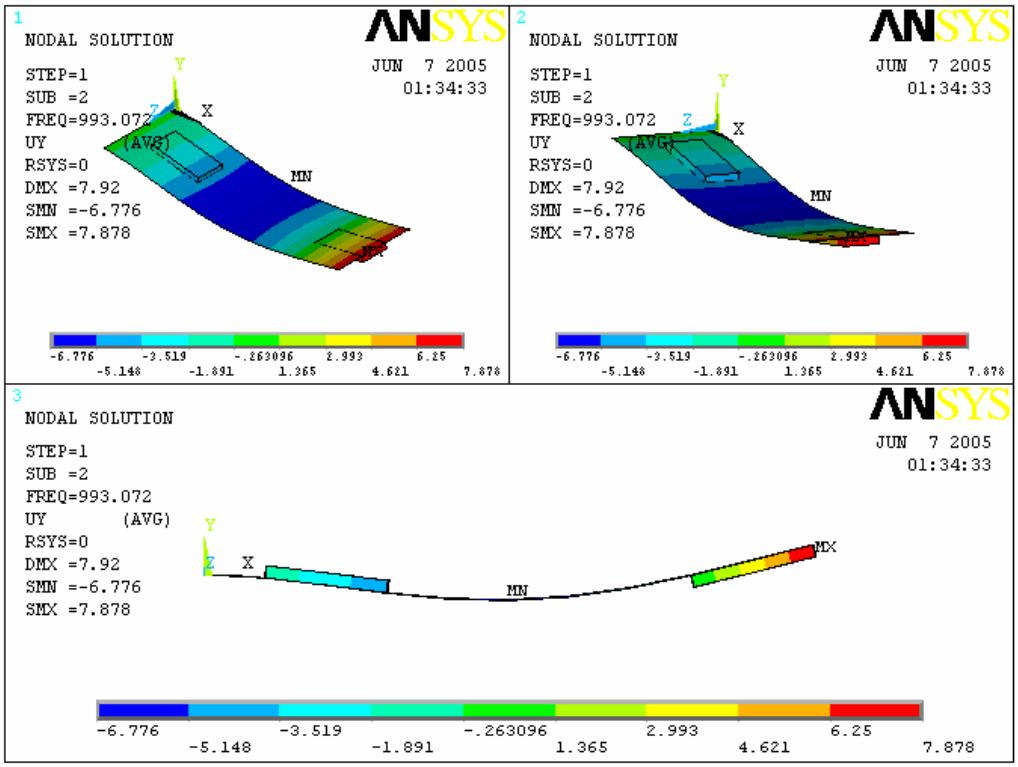

Figure 4.9 2nd mode shape for the plate with PZT's (PZT actuator placed at location 1).

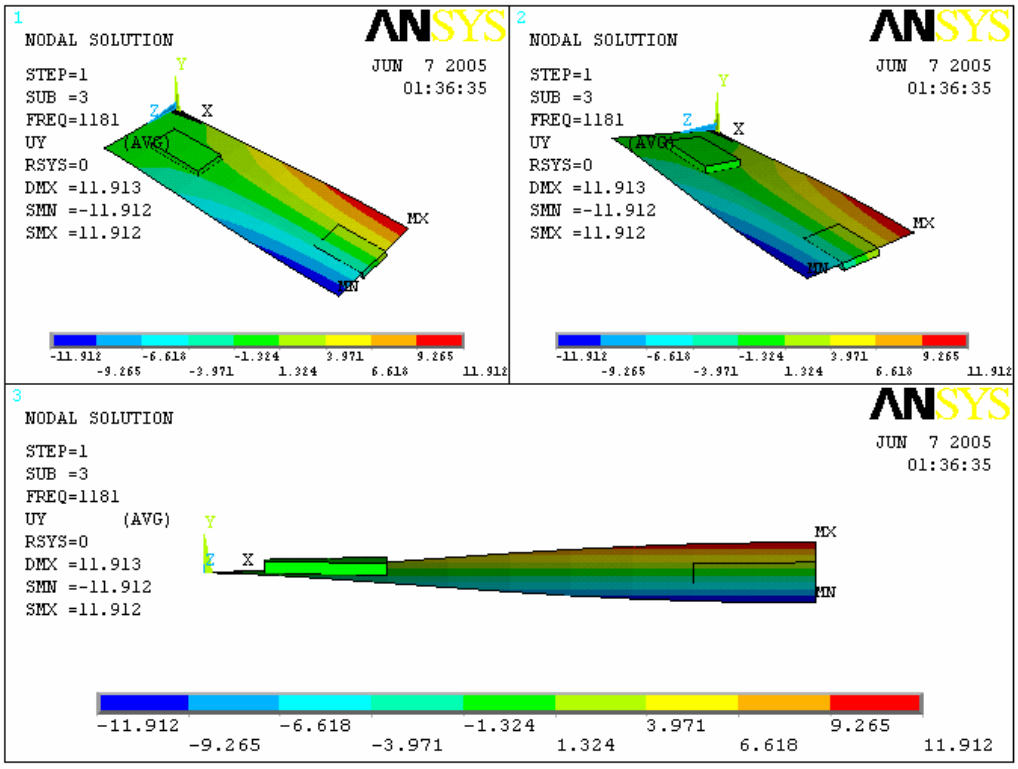

Figure 4.10 3rd mode shape for the plate with PZT's

(PZT actuator placed at location 1).

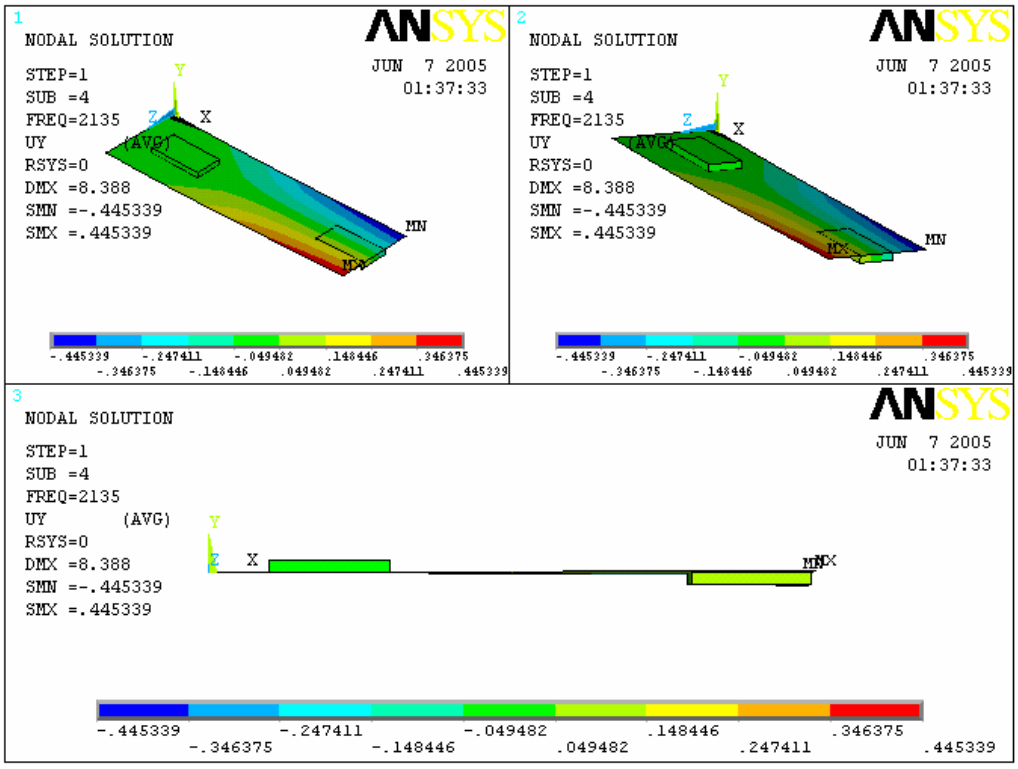

Figure 4.11 4th mode shape for the plate with PZT's

(PZT actuator placed at location 1).

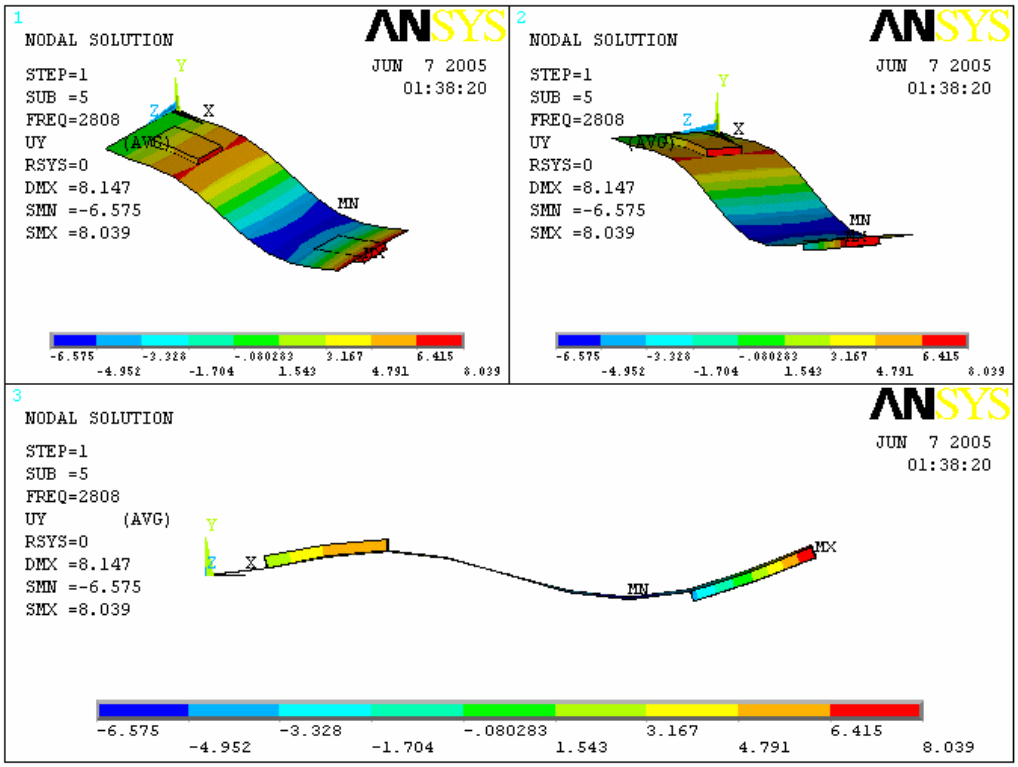

Figure 4.12 5th mode shape for the plate with PZT's (PZT actuator placed at location 1).

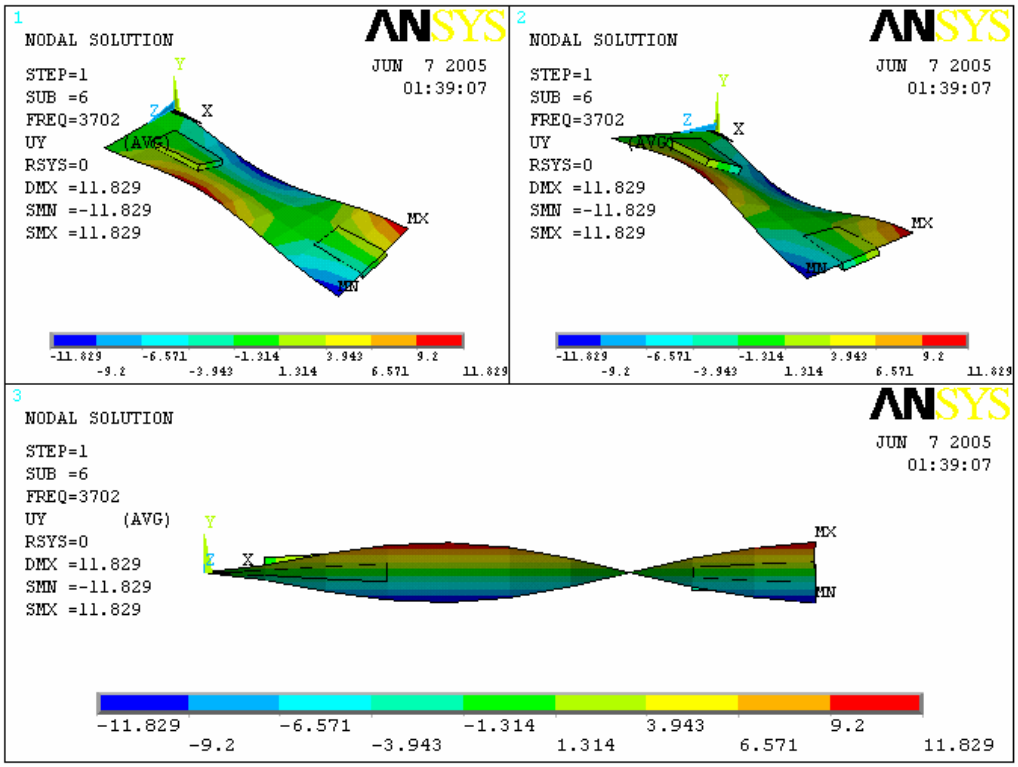

Figure 4.13 6th mode shape for the plate with PZT's

(PZT actuator placed at location 1).

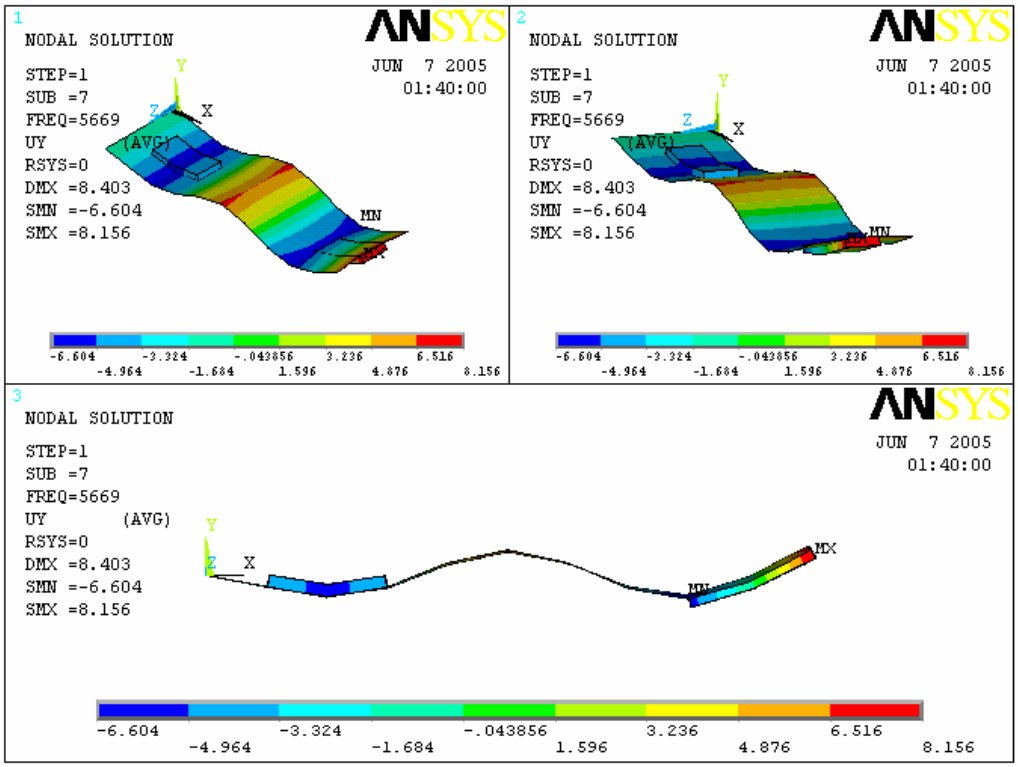

Figure 4.14 7th mode shape for the plate with PZT's

(PZT actuator placed at location 1).

TABLE 4.2 Transverse displacements for nodes 3 and 6 of the actuator for the first seven mode shapes of the beam with PZT's. (Location 1)

Mode Shape	**Frequency (Hz)**	**Node #**	**Displacement**
1st mode	159.105	3	1.1435
1st mode	159.105	6	1.1435
2nd mode	999.072	3	-4.6965
2nd mode	999.072	6	-4.6965
3rd mode	1181	3	-1.3187
3rd mode	1181	6	1.3187
4th mode	2135	3	0.0039460
4th mode	2135	6	-0.0039460
5th mode	2808	3	6.4518
5th mode	2808	6	6.4518
6th mode	3702	3	3.5289
6th mode	3702	6	-3.5289
7th mode	5669	3	-3.5101
7th mode	5669	6	-3.5101

TABLE 4.3 Transverse displacements for nodes 3 and 6 of the actuator for the first seven mode shapes of the beam with PZT's. (Location 2)

Mode Shape	**Frequency (Hz)**	**Node #**	**Displacement**
1st mode	154.22	3	2.8706
1st mode	154.22	6	2.8706
2nd mode	983.45	3	-6.1449
2nd mode	983.45	6	-6.1449
3rd mode	1175.6	3	-2.4985
3rd mode	1175.6	6	2.4985
4th mode	2118.6	3	-0.075614
4th mode	2118.6	6	0.075614
5th mode	2848.9	3	0.069349
5th mode	2848.9	6	0.069349
6th mode	3616.9	3	3.2427
6th mode	3616.9	6	-3.2427
7th mode	5651.7	3	6.2278
7th mode	5651.7	6	6.2278

TABLE 4.4 Transverse displacements for nodes 3 and 6 of the actuator for the first seven mode shapes of the beam with PZT's. (Location 3)

Mode Shape	**Frequency (Hz)**	**Node #**	**Displacement**
1st mode	149.37	3	4.8774
1st mode	149.37	6	4.8774
2nd mode	1006.5	3	2.9008
2nd mode	1006.5	6	2.9008
3rd mode	1153.3	3	-3.3363
3rd mode	1153.3	6	3.3363
4th mode	2079.6	3	0.0437
4th mode	2079.6	6	-0.0437
5th mode	2881.3	3	5.5822
5th mode	2881.3	6	5.5822
6th mode	3757.4	3	-0.037347
6th mode	3757.4	6	0.037347
7th mode	5660.6	3	-3.2089
7th mode	5660.6	6	-3.2089

TABLE 4.5 Transverse displacements for nodes 3 and 6 of the actuator for the first seven mode shapes of the beam with PZT's. (Location 4)

Mode Shape	**Frequency (Hz)**	**Node #**	**Displacement**
1st mode	158.55	3	1.1457
1st mode	158.55	6	1.1105
2nd mode	993.06	3	-4.7379
2nd mode	993.06	6	-4.9304
3rd mode	1172.8	3	1.2876
3rd mode	1172.8	6	3.8390
4th mode	2162.3	3	0.28282
4th mode	2162.3	6	0.35587
5th mode	2795.9	3	6.65
5th mode	2795.9	6	7.6441
6th mode	3581	3	-2.4198
6th mode	3581	6	-8.93
7th mode	5659.1	3	-3.3311
7th mode	5659.1	6	-3.9357

TABLE 4.6 Transverse displacements for nodes 3 and 6 of the actuator for the first seven mode shapes of the beam with PZT's. (Location 5)

Mode Shape	**Frequency (Hz)**	**Node #**	**Displacement**
1st mode	153.88	3	2.8688
1st mode	153.88	6	2.8449
2nd mode	975	3	-6.3801
2nd mode	975	6	-7.4088
3rd mode	1150.4	3	1.0753
3rd mode	1150.4	6	5.7993
4th mode	2127.4	3	-0.11633
4th mode	2127.4	6	-0.21332
5th mode	2838.4	3	0.13037
5th mode	2838.4	6	0.54378
6th mode	3432.1	3	-1.9742
6th mode	3432.1	6	-7.7075
7th mode	5643.4	3	6.1989
7th mode	5643.4	6	6.6532

TABLE 4.7 Transverse displacements for nodes 3 and 6 of the actuator for the first seven mode shapes of the beam with PZT's. (Location 6)

Mode Shape	**Frequency (Hz)**	**Node #**	**Displacement**
1st mode	149.29	3	4.88
1st mode	149.29	6	4.8737
2nd mode	987.46	3	-3.5840
2nd mode	987.46	6	-5.8057
3rd mode	1112.6	3	1.6176
3rd mode	1112.6	6	7.5023
4th mode	2078.6	3	0.018112
4th mode	2078.6	6	-0.056176
5th mode	2876.9	3	-5.3690
5th mode	2876.9	6	-5.6585
6th mode	3674.9	3	1.0203
6th mode	3674.9	6	0.94398
7th mode	5658.6	3	-3.3135
7th mode	5658.6	6	-3.7517

4.3 CASE 1: LQR CONTROLLER

For the six different PZT actuator locations shown in Figure 4.7, an LQR controller will be added to the system. The effect of changing the actuator location on controlling the structural vibrations will be tested. The output voltage will be taken from two nodes instead of one node. The output will be measured from nodes 9 and 12 of the sensor, and then will be fed from the controller to nodes 1 and 4 of the actuator respectively.

The eigenvalues of the closed-loop state matrix of Eq. (3.12) are computed and shown in Figure 4.15. The figure clearly shows that the system is stable since there are no eigenvalues that lie in the right hand side plane.

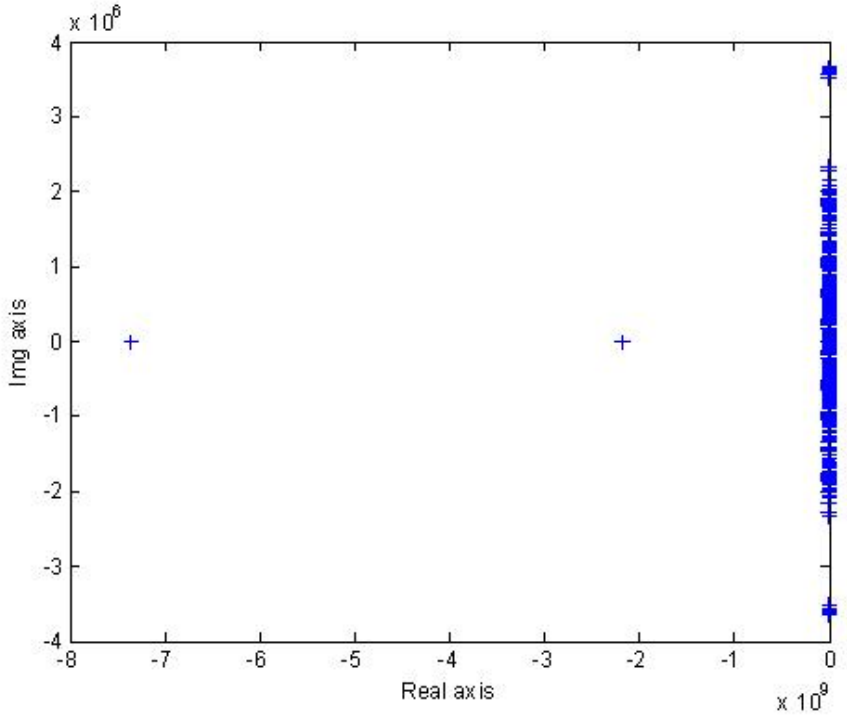

Figure 4.15 Closed-loop eigenvalues for the plate and PZT's with LQR controller.

The weighting matrices for the LQR controller are taken as follows; Q = 10^{-4} x I (2 x ndof) and R = 10^{-6} x I (2). The voltages output for the six actuator locations are shown and discussed in the results.

4.4 CASE 2: LQG CONTROLLER

An LQG controller will be added to the system in this case. The same actuator locations used in case 1 will be used for the analysis. The output voltages are also going to be measured from nodes 9 and 12 of the sensor. The closed-loop eigenvalues are shown in Figure 4.16 for the plate with PZT's system with LQG controller.

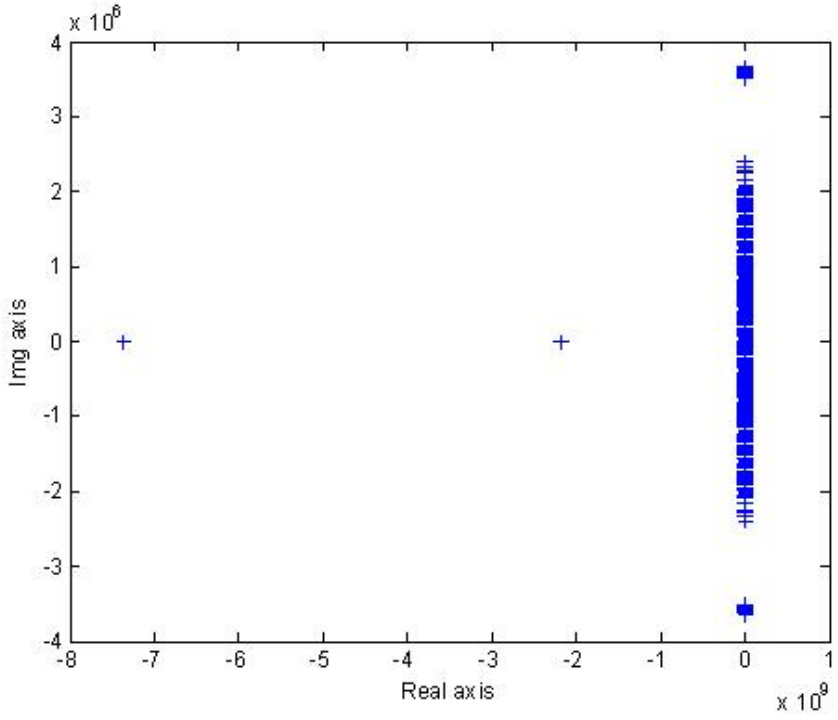

Figure 4.16 Closed-loop eigenvalues for the plate and PZT's with LQR controller.

The weighting matrices for the LQR part of the LQG controller are taken as Q = 10^{-4} x I (2 x nodf) and R = 10^{-6} x I (2). The weighting matrices for the Kalman estimator, Qe and Re, are taken as 10^{-2} x I (3) and 10^{-6} x I (2) respectively.

4.5 RESULTS and DISCUSSION

4.5.1 CASE 1: LQR CONTROLLER

Figures 4.17 – 4.22, show the sensor voltages outputs for the six different locations of the actuator. The output voltages are measured from nodes 9 and 12 of the sensor as we mentioned before. Output (1) refers to node 9, and output (2) refers to node 12.

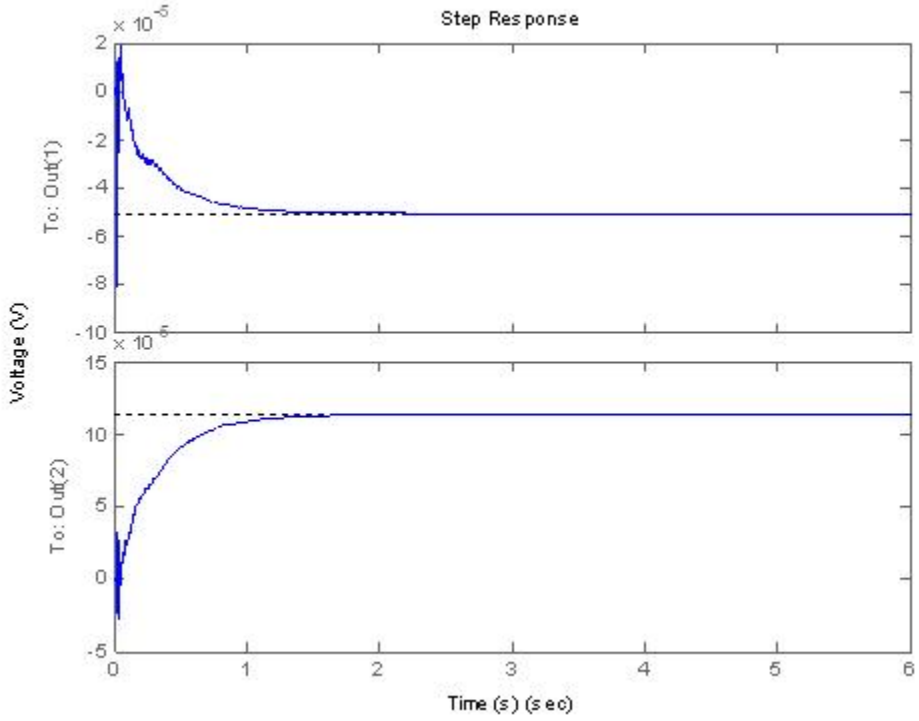

Figure 4.17 Closed-loop sensor voltages (PZT actuator placed at location 1) with an LQR controller.

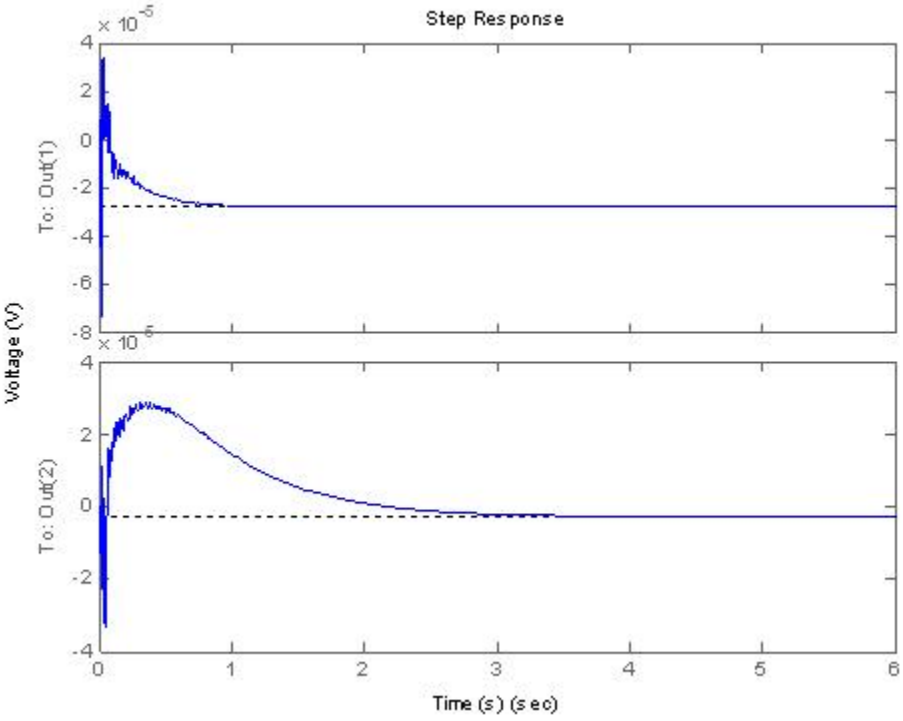

Figure 4.18 Closed-loop sensor voltages (PZT actuator placed at location 2) with an LQR controller.

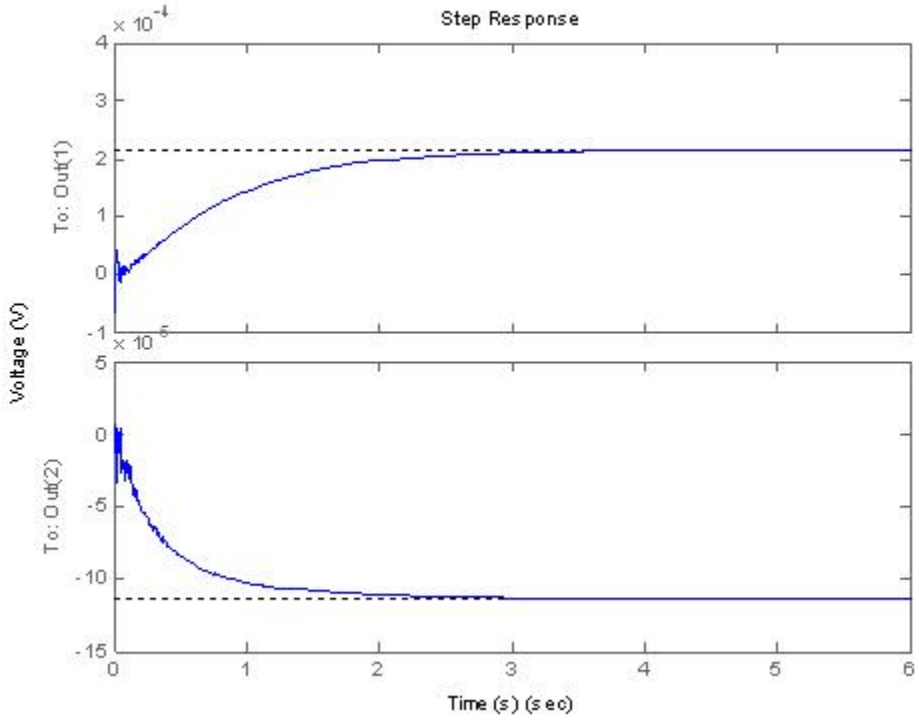

Figure 4.19 Closed-loop sensor voltages (PZT actuator placed at location 3) with an LQR controller.

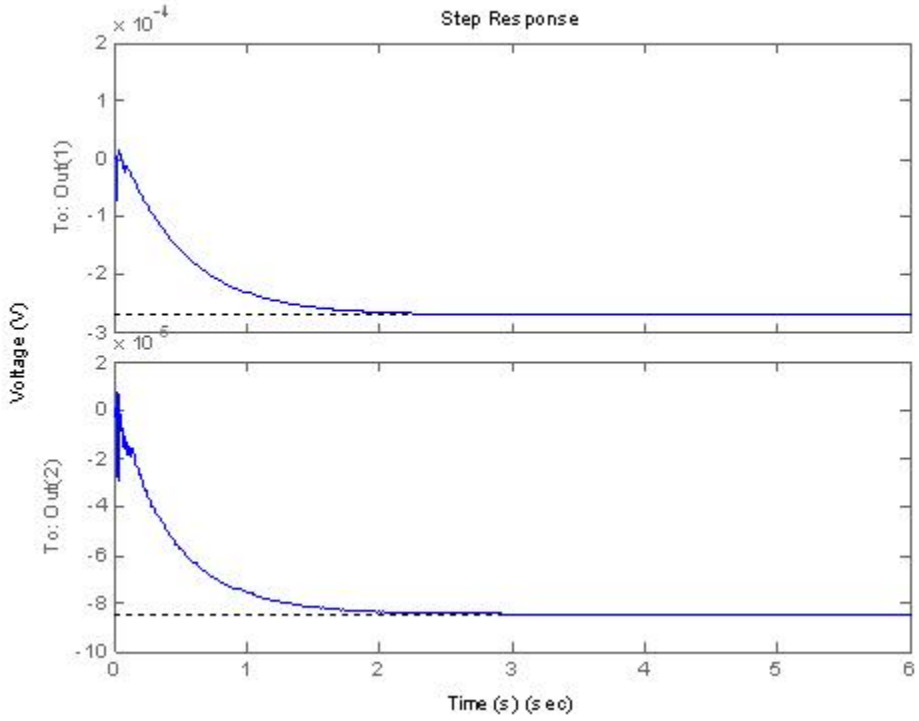

Figure 4.20 Closed-loop sensor voltages (PZT actuator placed at location 4) with an LQR controller.

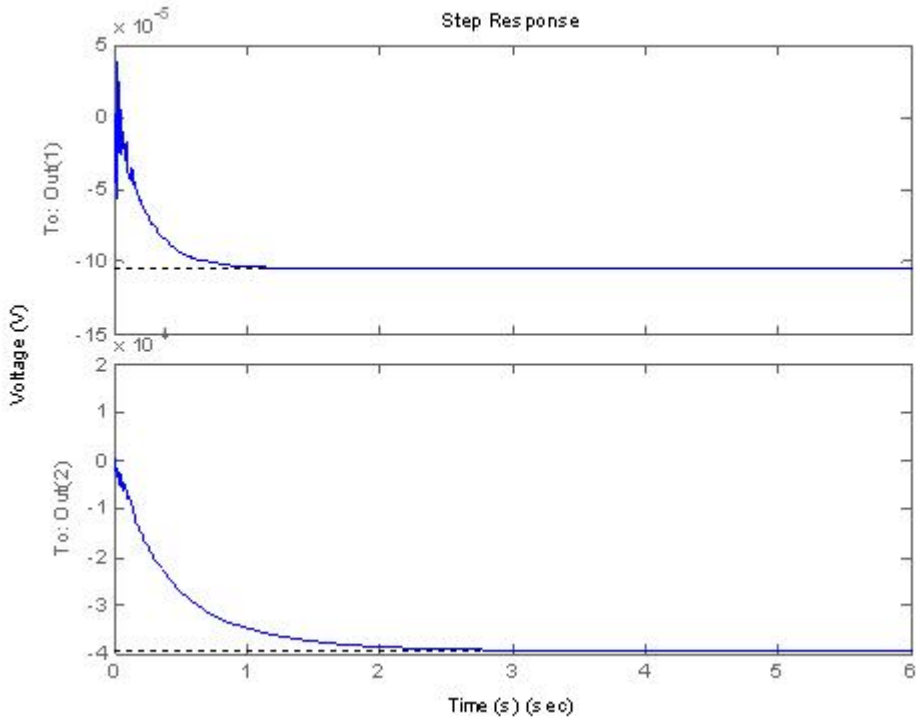

Figure 4.21 Closed-loop sensor voltages (PZT actuator placed at location 5) with an LQR controller.

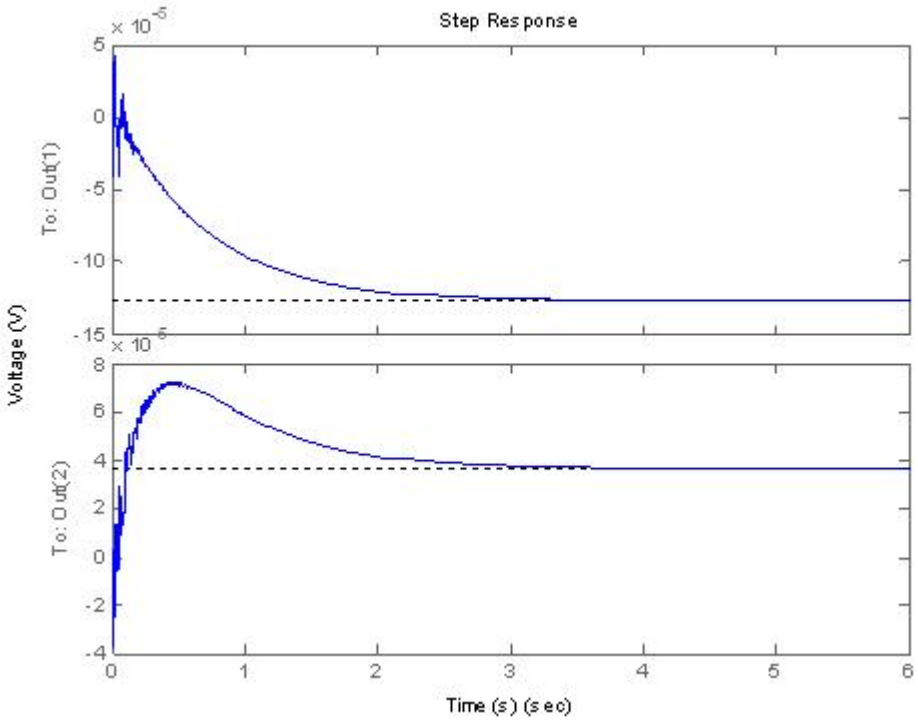

Figure 4.22 Closed-loop sensor voltages (PZT actuator placed at location 6) with an LQR controller.

One can see from the output voltages, the behavior in the case of the plate with PZT's is different from the case with the beam structure. First we have varied the location of the actuator in two directions rather than one, as in the beam case. Second, the outputs and the inputs are measured and fed to two nodes for the sensor and the actuator.

Due to the symmetry of the problem, since we have two unit step forces applied at the tip of the plate, the reading from node 9 of the sensor is the same for the actuator locations that are varied along the width of the plate. That can be observed from the reading of output (1) for the actuator locations 1 and 4 in Figures 4.17 and 4.20, 2 and 5 in Figures 4.18 and 4.21, and for locations 3 and 6 in Figures 4.19 and 4.22.

Now, considering the output of node 9, output (1). Varying the actuator location along the length of the plate shows that the settling time has the best values when the actuator is placed at locations 2 and 5. Also it can be seen that the settling time value is better in the actuator locations 1 and 4 than locations 3 and 6. In general, it can be said that placing the actuator closer to the fixed side of the plate gives better results than placing it closer to the free end.

For the output of node 12, output (2), a similar behavior to node 9 can be observed except for actuator location 2. For the other five locations of the actuator, the behavior is the same as node 9.

The effect of varying the actuator location along the width can be observed only for the output of node 12 because the output of node 9 is the same due to the symmetry as we mentioned. If we compare the output of node 12 for the actuator locations 1-6, one can see that the settling time is smaller for the locations 1 and 3 than the locations 4 and 5, except for location 2 and 5. So it can be said in general that placing the actuator closer to the center of the plate gives better results in terms of the settling time.

Combining all the effects mentioned, one can see that the PZT actuator performs better in attenuating the structural vibrations as we place it closer to the center of the plate. Also it is important to notice that placing the actuator closer to the fixed side of the plate gives good results compared to locations other than the center.

4.5.2 CASE 2: LQG CONTROLLER

Figures 4.23 – 4.28, shows the voltages output for the six different locations of the PZT actuator. The output voltage is measured from nodes 9, output (1) in the figures, and 12, output (2) in the figures, of the sensor.

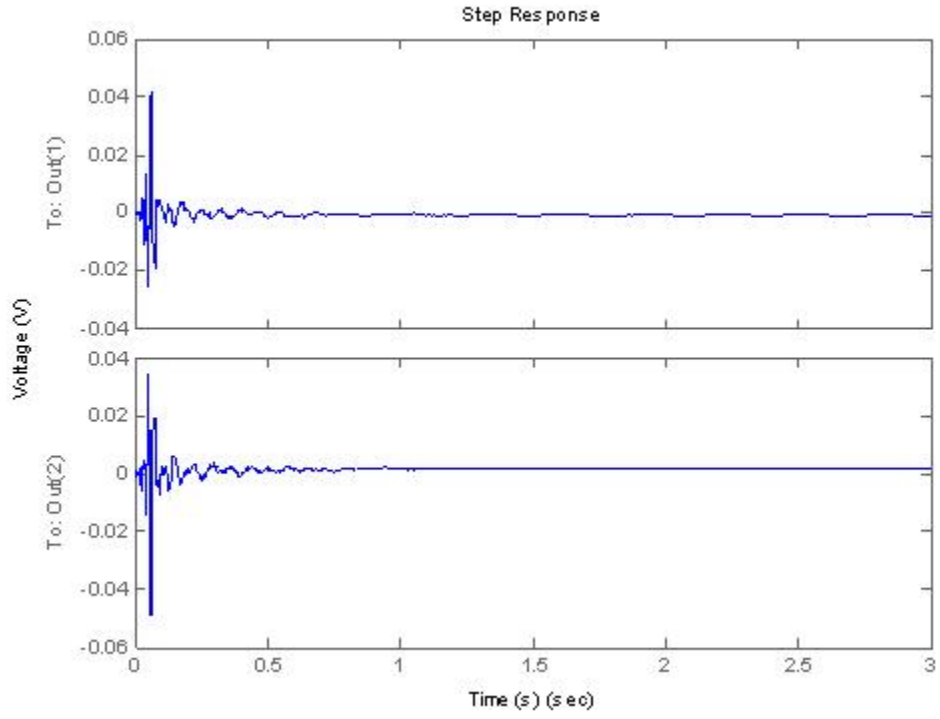

Figure 4.23 Closed-loop sensor voltages (PZT actuator placed at location 1) with an LQG controller.

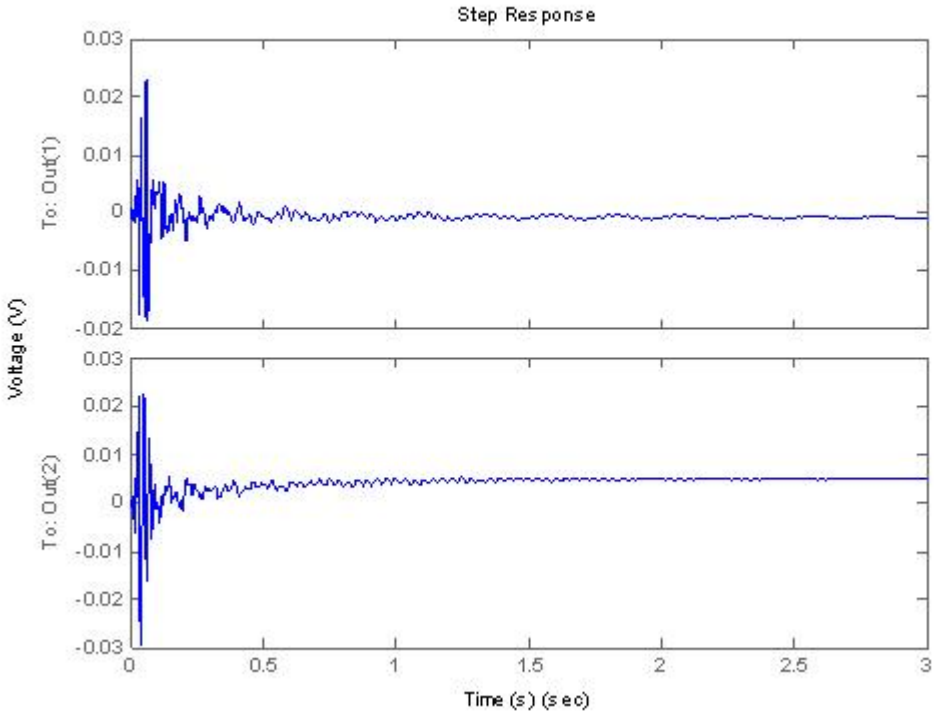

Figure 4.24 Closed-loop sensor voltages (PZT actuator placed at location 2) with an LQG controller.

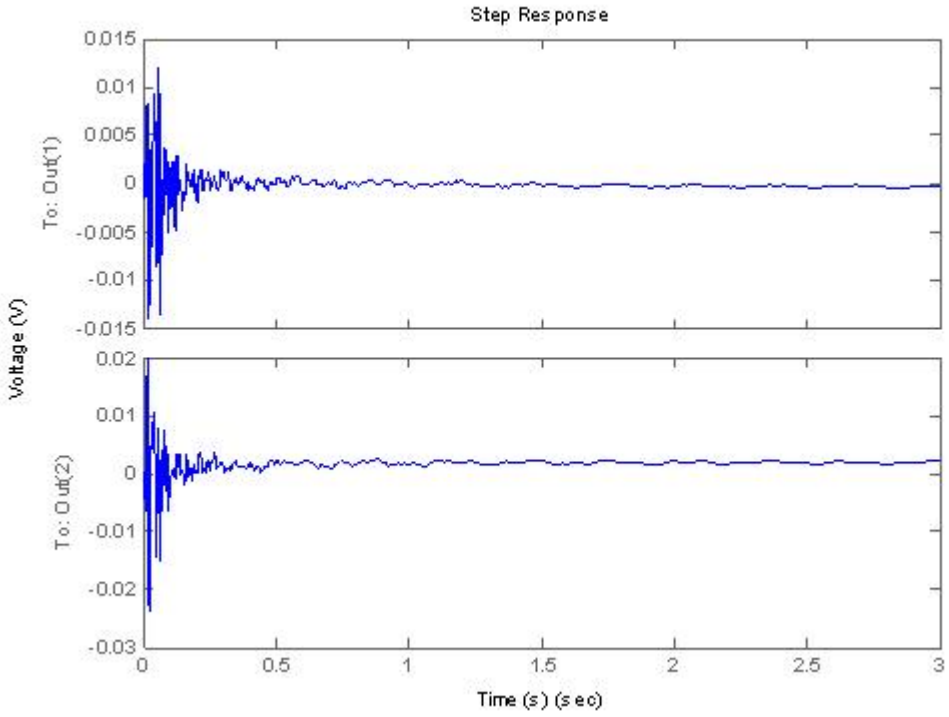

Figure 4.25 Closed-loop sensor voltages (PZT actuator placed at location 3) with an LQG controller.

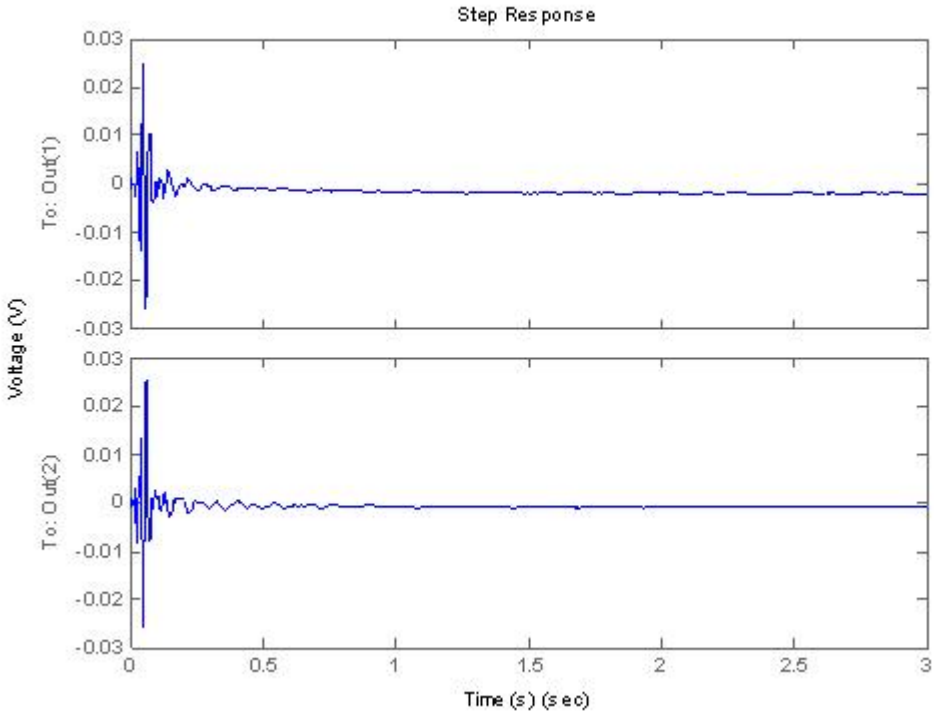

Figure 4.26 Closed-loop sensor voltages (PZT actuator placed at location 4) with an LQG controller.

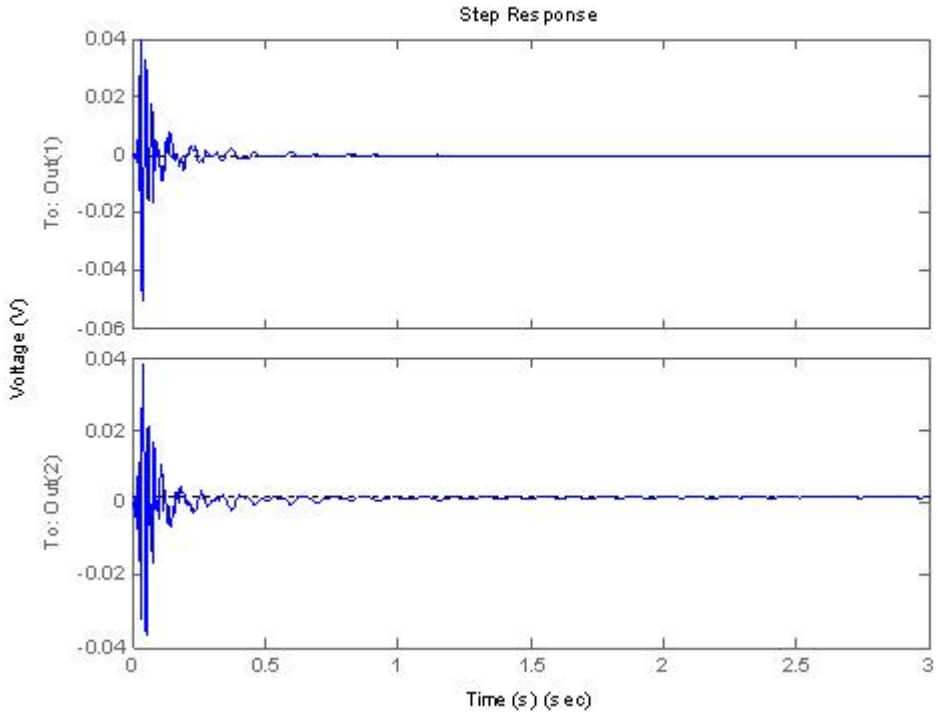

Figure 4.27 Closed-loop sensor voltages (PZT actuator placed at location 5) with an LQG controller.

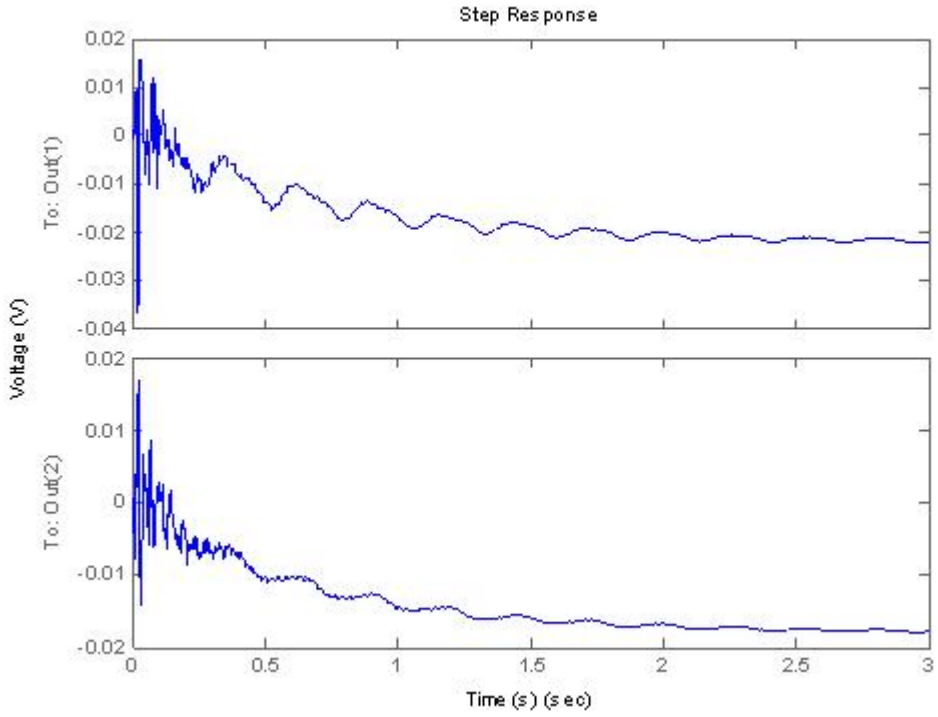

Figure 4.28 Closed-loop sensor voltages (PZT actuator placed at location 6) with an LQG controller.

By looking at the outputs reading from both nodes, 9 and 12, it is clear that moving the actuator far from the fixed end side of the plate increases the settling time. This can be observed by looking to the settling time values for actuator locations 1-3, and 4-5.

Now, if we compare the output reading of node 12, output (2), for the settling time between the actuator locations 1 and 4, Figures 4.23 and 4.26, for locations 1 it takes about 1.1 sec to reach a stable state, whereas it takes about 1.9 sec when the actuator is placed at location 4. Note that the output of node 9, output (1), gives the same reading in both locations. For locations 2 and 5, Figures 4.24 – 4.27, the output of node 9, output (1), shows that location 5 gives better results in terms of the settling time, whereas the output of node 12, output (2), shows the opposite of that. For the same two locations, 2 and 5, if we look at the vibration peaks, we can see that placing the actuator towards the center reduces the values for these peaks. Finally, comparing the locations 3 and 6, Figures 4.25 – 4.28, it is clear that location 3 shows better settling time than location 6, whereas the vibration peaks are reduced if we look to output (1). It is important to state that the steady state values for location 3 are close to zero, whereas they are not for location 6.

From this case, one can see that placing the actuator closer to the fixed end of the plate, in terms of the length, and closer to the center, in terms of the width, controls the structural vibrations better than placing it far from the fixed end and towards the edges.

CHAPTER 5

CONCLUSIONS AND RECOMMENDATIONS

5.1 CONCLUSIONS

In this work, a comprehensive study is done for the effect of the piezoelectric actuator placement on controlling the structural vibrations. Two systems were used for this study, the first one was a 2-D beam with PZT actuator and sensor, and the second one was a 3-D plate with PZT actuator and sensor. Both systems were modeled in MATLAB. For each model, two types of controllers were applied, an LQR and an LQG controllers.

The finite element formulations for the PZT's, beam and plate were discussed. The materials used in both systems were the same. The PZT's material used is BM500, whereas the beam and plate were steel.

The models for each system were checked by comparing the output voltages of the PZT's with another model that was done in ANSYS. Results were satisfying, and our MATLAB model showed similar results to the one obtained from ANSYS.

The actuator node(s) where we feed the input voltages was checked at each actuator location that is it not located at any modal nodes. All the cases, for both

systems, showed that our actuator locations used for the study were acceptable since the feeding node had transverse displacement values that were not zero. For the 2-D beam, the modal nodes were checked up to the 3rd mode shape, whereas for the 3-D plate we checked up to the 7th mode shape.

The beam with PZT's system showed clearly that as we place the actuator closer to the fixed end of the beam we get better results in controlling the structural vibrations in terms of the settling time. This was observed with the two controllers, the LQR and the LQG.

For the plate with PZT's system, the actuator location was varied along the length and the width of the plate. For the case with the LQR controller, the settling time for the actuator locations between the center and the fixed side of the plate along the length gave better results in attenuating the structural vibrations. Along the width of the plate, placing the actuator at the center showed better results for the settling time too. For the LQG controller, placing the actuator closer to the fixed side performs better in terms of the settling time. The peaks of the vibration were less for the cases where we placed the actuator at the center of the plate in terms of the width.

5.2 RECOMMENDATIONS

Even though this work has a comprehensive 2-D and 3-D study for the effect of the PZT actuator placement on controlling the vibrations, but there are many things that are not done yet.

In this study, the actuator locations were checked so that the actuator nodes are not placed at any modal node, whereas the effect was studied regarding the actuator's location only. Another direction is that to study the effect of the actuator placement in terms of the modal nodes at every mode shape. Placing the PZT actuator closer to any of the modal nodes could have some interesting results.

Also one can extend the study for different structures, such as circular disks and tapered beams. For these shapes, the conclusion might be different from the beam, either 2-D or 3-D.

Different excitation forces can be used to generalize the conclusion. Also other types of controllers can be applied to the system consisting of the structure and the PZT's.

APPENDIX

I. PROGRAMING FLOW CHART

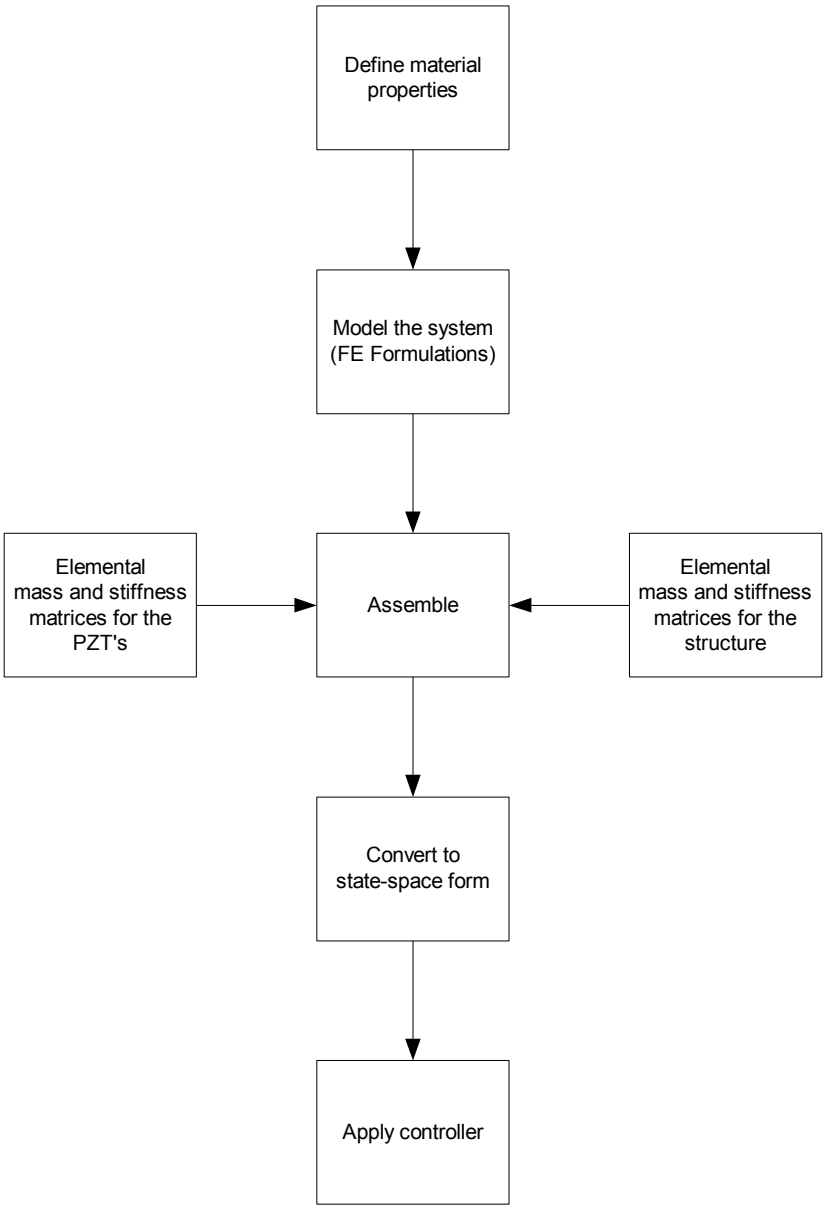

II. PROGRAM EXAMPLE

BEAM WITH PZT'S

CASE 1: LQR CONTROLLER **(Actuator placed 5 mm from fixed end)**

Defining material properties:

```
rhop=7500;ep=1.21e11;
rhos=7800;es=2.07e11;anus=0.3;
el31o=[-5.4*ones(1,4)];el33o=[15.8*ones(1,4)];el15o=[12.3*ones(1,4)];
eps11=1.151e-3;eps33=1.043e-3;
e11n(1:4)=11.1e10*ones(1,4);
e12n(1:4)=7.52e10*ones(1,4);
e22n(1:4)=12.1e10*ones(1,4);
e33n(1:4)=2.26e10*ones(1,4);
```

Modeling the system (FE Formulations):

```
len=[0.005*ones(1,1),lp*ones(1,4),0.005*ones(1,10),lp*ones(1,4),0.005*ones(1,1)];
%PZ act dofv num
nelcaf=[30,30,2,1;30,30,3,2;30,30,4,3;30,30,5,4];
%PZ sen dofv num
nelcaf2=[6,7,30,30;7,8,30,30;8,9,30,30;9,10,30,30];
%PZ act dof num
idenp=[21,22,24,25,3,4,1,2;24,25,27,28,5,6,3,4;27,28,30,31,7,8,5,6;30,31,33,34,9,10,7,8];
%PZ sen dof num
idenp2=[11:14,66,67,63,64;13:16,69,70,66,67;15:18,72,73,69,70;17:20,75,76,72,73];
%structure dof num
```

```
idens=[200*ones(1,3),21:23;21:26;24:29;27:32;30:35;33:38;36:41;39:44;42:47;45:50;48:53;
   51:56;54:59;57:62;60:65;63:68;66:71;69:74;72:77;75:80];
```

Assembling:

```
e(1:nelemp)=ep*ones(1,nelemp);anu(1:nelemp)=anup*ones(1,nelemp);
i=1;
while i<= nelemp
epss(i)=e(i)/(1-anu(i)*anu(i));pss1(i)=0.5*(1-anu(i));
epst(i)=e(i)/(1+anu(i))/(1-2*anu(i));e11n(i)=epss(i);
pst1(i)=1-anu(i);pst2(i)=0.5*(1-2*anu(i));e22n(i)=epss(i);
e12n(i)=epss(i)*anu(i);e33n(i)=epss(i)*pss1(i);
i=i+1;
end
i=1;
while i <= ndof
j=1;
while j <= ndof
kuu(i,j)=0;
muu(i,j)=0;
j=j+1;
end
i=i+1;
end
i=1;
while i <= ndof
j=1;
while j <= nvolt
kuf(i,j)=0;
```

```
j=j+1;
end
i=i+1;
end
i=1;
while i <= nvolt
j=1;
while j <= nvolt
kff(i,j)=0;
j=j+1;
end
i=i+1;
end
n=1;
while n <= nelemp
e11=e11n(n);
e22=e22n(n);
e12=e12n(n);
e33=e33n(n);

[kuuel,muuel]=elemsa(ap,bp,w,rhop,e11,e22,e12,e33);
i=1;
while i <= 8
i1=idenp(n,i);
while i1 <= ndof
j=1;
while j <= 8
j1=idenp(n,j);
```

```
while j1 <= ndof
kuu(i1,j1)=kuu(i1,j1)+kuuel(i,j);
muu(i1,j1)=muu(i1,j1)+muuel(i,j);
j1=ndof+1;
end
j=j+1;
end
i1=ndof+1;
end
i=i+1;
end
n=n+1;
end

%Assemblage of kuu and Muu matrices
n=1;
while n <= nelemp
e11=e11n(n);
e22=e22n(n);
e12=e12n(n);
e33=e33n(n);
[kuuel,muuel]=elemsa(ap,bp,w,rhop,e11,e22,e12,e33);
i=1;
while i <= 8
i1=idenp2(n,i);
while i1 <= ndof
j=1;
while j <= 8
```

```
j1=idenp2(n,j);
while j1 <= ndof
kuu(i1,j1)=kuu(i1,j1)+kuuel(i,j);
muu(i1,j1)=muu(i1,j1)+muuel(i,j);
j1=ndof+1;
end
j=j+1;
end
i1=ndof+1;
end
i=i+1;
end
n=n+1;
end

n=1;
while n <= nelems
leng=len(n);
[kuuel,muuel]=beamt(es,xi,leng,area,rhos);
i=1;
while i <= 6
i1=idens(n,i);
while i1 <= ndof
j=1;
while j <= 6
j1=idens(n,j);
while j1 <= ndof
kuu(i1,j1)=kuu(i1,j1)+kuuel(i,j);
```

```
muu(i1,j1)=muu(i1,j1)+muuel(i,j);
j1=ndof+1;
end
j=j+1;
end
i1=ndof+1;
end
i=i+1;
end
n=n+1;
end
%Assemblage of Kuf and Kff matrices
%%%% coupling for actuator %%%%
n=1;
while n <= nelemp
el31=el31o(n);
el33=el33o(n);
el15=0;
[kufel,kffel]=elemp(ap,bp,w,rhop,el15,el31,el33,eps11,eps33);
i=1;
while i <= 8
i1=idenp(n,i);
while i1 <= ndof
j=1;
while j <= 4
jaf=nelcaf(n,j);
while jaf <= nvolt
kuf(i1,jaf)=kuf(i1,jaf)+kufel(i,j);
```

```
jaf=nvolt+1;
end
j=j+1;
end
i1=ndof+1;
end
i=i+1;
end
i=1;
while i <= 4
iaf=nelcaf(n,i);
while iaf <= nvolt
j=1;
while j <= 4
jaf=nelcaf(n,j);
while jaf <= nvolt
kff(iaf,jaf)=kff(iaf,jaf)+kffel(i,j);
jaf=nvolt+1;
end
j=j+1;
end
iaf=nvolt+1;
end
i=i+1;
end
n=n+1;
end
```

```
%%%% coupling for sensor %%%%

n=1;

while n <= nelemp

el31=el31o(n);

el33=el33o(n);

el15=0;

[kufel,kffel]=elemp(ap,bp,w,rhop,el15,el31,el33,eps11,eps33);

i=1;

while i <= 8

i1=idenp2(n,i);

while i1 <= ndof

j=1;

while j <= 4

jaf=nelcaf2(n,j);

while jaf <= nvolt

kuf(i1,jaf)=kuf(i1,jaf)+kufel(i,j);

jaf=nvolt+1;

end

j=j+1;

end

i1=ndof+1;

end

i=i+1;

end

i=1;

while i <= 4

iaf=nelcaf2(n,i);

while iaf <= nvolt
```

```
j=1;
while j <= 4
jaf=nelcaf2(n,j);
while jaf <= nvolt
kff(iaf,jaf)=kff(iaf,jaf)+kffel(i,j);
jaf=nvolt+1;
end
j=j+1;
end
iaf=nvolt+1;
end
i=i+1;
end
n=n+1;
end
ak1=kuu+kuf*inv(kff)*kuf';
af=[zeros(1,78),1,0]';
u=inv(ak1)*af;
vstat=inv(kff)*kuf'*u;
E=zeros(10);E(1:nvolt,5)=1;
F=zeros(10);F(1:nvolt,10)=1;
C=0;
cuu=kuf*inv(kff)*E*C*F*inv(kff)*kuf';
```

Converting to state space form:

```
a=[zeros(ndof),eye(ndof);-inv(muu)*ak1,-inv(muu)*cuu];
bf=[0*af;inv(muu)*af];
c=[eye(ndof),zeros(ndof)];
```

```
d=[zeros(ndof,1)];

b=[0*kuf*inv(kff);inv(muu)*kuf*inv(kff)];
```

Applying controller:

```
q=0.0000001*eye(2*ndof);r=eye(nvolt);

kk=lqr(a,b,q,r);

acl=a-b*kk;

t=0:0.0001:6;

y=step(acl,bf,c,d,1,t);
```

Subroutines:

function [akel,amuuel]=elemsa(a,b,t,rho,e11,e22,e12,e33)

```
    s1=t*b*e11/6./a;

    s2=t*a*e22/6./b;

    s3=t*e12/4.;

    s4=t*a*e33/6./b;

    s5=t*b*e33/6./a;

    s6=t*e33/4.;

    akel(1,1)=2.*(s1+s4);

    akel(2,1)=s3+s6;

    akel(2,2)=2.*(s2+s5);

    akel(3,1)=s4-2.*s1;

    akel(3,2)=s6-s3;

    akel(3,3)=2.*(s1+s4);

    akel(4,1)=s3-s6;

    akel(4,2)=s2-2.*s5;

    akel(4,3)=-s3-s6;
```

```
akel(4,4)=2.*(s2+s5);

akel(5,1)=-s1-s4;

akel(5,2)=-s3-s6;

akel(5,3)=s1-2.*s4;

akel(5,4)=s6-s3;

akel(5,5)=2.*(s1+s4);

akel(6,1)=-s3-s6;

akel(6,2)=-s2-s5;

akel(6,3)=s3-s6;

akel(6,4)=s5-2.*s2;

akel(6,5)=s3+s6;

akel(6,6)=2.*(s2+s5);

akel(7,1)=s1-2.*s4;

akel(7,2)=s3-s6;

akel(7,3)=-s1-s4;

akel(7,4)=s3+s6;

akel(7,5)=s4-2.*s1;

akel(7,6)=s6-s3;

akel(7,7)=2.*(s1+s4);

akel(8,1)=s6-s3;

akel(8,2)=s5-2.*s2;

akel(8,3)=s3+s6;

akel(8,4)=-s2-s5;

akel(8,5)=s3-s6;

akel(8,6)=s2-2.*s5;

akel(8,7)=-s3-s6;

akel(8,8)=2.*(s2+s5);

i=1;
```

```
while i <= 8
j=1;
while j <= 8
if i > j
akel(j,i)=akel(i,j);
end
j=j+1;
end
i=i+1;
end
i=1;
while i <= 8
j=1;
while j <= 8
akeln(i,j)=0;
j=j+1;
end
i=i+1;
end
akeln(1,1)=1;
akeln(3,1)=-1;
akeln(5,1)=1;
akeln(7,1)=-1;
akeln(1,3)=-1;
akeln(3,3)=1;
akeln(5,3)=-1;
akeln(7,3)=1;
akeln(1,5)=1;
```

```
akeln(3,5)=-1;

akeln(5,5)=1;

akeln(7,5)=-1;

akeln(1,7)=-1;

akeln(3,7)=1;

akeln(5,7)=-1;

akeln(7,7)=1;

say=t*(e33*a*a+e12*e12*b*b/e22)/12./a/b;

i=1;

while i <= 8

j=1;

while j <= 8

akeln(i,j)=say*akeln(i,j);

j=j+1;

end

i=i+1;

end

i=1;

while i <= 8

j=1;

while j <= 8

akels(i,j)=akel(i,j)-akeln(i,j);

j=j+1;

end

i=i+1;

end

i=1;

while i <= 8
```

```
j=1;
while j <= 8
amuuel(i,j)=0;
j=j+1;
end
i=i+1;
end
i=1;
while i <= 8
amuuel(i,i)=4;
i=i+1;
end
i=1;
while i <= 6
amuuel(i+2,i)=2;
amuuel(i,i+2)=2;
i=i+1;
end
i=1;
while i <= 4
amuuel(i+4,i)=1;
amuuel(i,i+4)=1;
i=i+1;
end
i=1;
while i <= 2
amuuel(i+6,i)=2;
amuuel(i,i+6)=2;
```

```
i=i+1;
end
amass=rho*a*b*t/9;
i=1;
while i <= 8
j=1;
while j <= 8
amuuel(i,j)=amass*amuuel(i,j);
j=j+1;
end
i=i+1;
end
```

function [k,m]=beamt(el,xi,leng,area,rho)

```
%-------------------------------------------------------------------
%  Purpose:
%     Stiffness and mass matrices for Hermitian beam element with axial DOF
%     nodal dof {v_1 theta_1 v_2 theta_2}
%
%  Synopsis:
%     [k,m]=beam_truss(el,xi,leng,area,rho)
%
%  Variable Description:
%     k - element stiffness matrix (size of 4x4)
%     m - element mass matrix (size of 4x4)
%     el - elastic modulus
%     xi - second moment of inertia of cross-section
```

```
%     leng - element length
%     area - area of beam cross-section
%     rho - mass density (mass per unit volume)
%-------------------------------------------------------------------

% stiffness matrix

 c=el*xi/(leng^3); c1=area*el/leng;
 k=[c1     0          0       -c1     0          0;...
    0    12*c      6*leng*c    0   -12*c       6*leng*c;...
    0    6*leng*c  4*c*leng^2  0   -6*c*leng   2*c*leng^2;...
    -c1    0          0        c1     0          0;...
    0    -12*c     -6*leng*c   0    12*c      -6*leng*c;...
    0    6*leng*c  2*c*leng^2  0   -6*leng*c   4*c*leng^2];

% consistent mass matrix

   mm=rho*area*leng/420;
   m=mm*[140  0          0          70        0        0;...
        0    156       22*leng     0         54       -13*leng;...
        0    22*leng   4*leng^2    0         13*leng  -3*leng^2;...
        70   0         0           140       0         0;...
        0    54        13*leng     0         156       -22*leng;...
        0    -13*leng  -3*leng^2   0         -22*leng  4*leng^2];
```

function [akufel,akffel]=elemp(a,b,t,rhop,el15,el31,el33,eps11,eps33)

```
c1=b/a/3;
c2=a/b/3;
c3=b/a/6;
c4=a/b/6;
akufel(1,1)=0.25*(el15+el31);
akufel(1,2)=0.25*(-el15+el31);
akufel(1,3)=-0.25*(el15+el31);
akufel(1,4)=0.25*(el15-el31);
akufel(2,1)=c1*el15+c2*el33;
akufel(2,2)=-c1*el15+c4*el33;
akufel(2,3)=-c3*el15-c4*el33;
akufel(2,4)=c3*el15-c2*el33;
akufel(3,1)=0.25*(el15-el31);
akufel(3,2)=-0.25*(el15+el31);
akufel(3,3)=0.25*(-el15+el31);
akufel(3,4)=0.25*(el15+el31);
akufel(4,1)=-c1*el15+c4*el33;
akufel(4,2)=c1*el15+c2*el33;
akufel(4,3)=c3*el15-c2*el33;
akufel(4,4)=-c3*el15-c4*el33;
akufel(5,1)=-0.25*(el15+el31);
akufel(5,2)=0.25*(el15-el31);
akufel(5,3)=0.25*(el15+el31);
akufel(5,4)=0.25*(-el15+el31);
akufel(6,1)=-c3*el15-c4*el33;
akufel(6,2)=c3*el15-c2*el33;
akufel(6,3)=c1*el15+c2*el33;
```

```
akufel(6,4)=-c1*el15+c4*el33;

akufel(7,1)=0.25*(-el15+el31);

akufel(7,2)=0.25*(el15+el31);

akufel(7,3)=0.25*(el15-el31);

akufel(7,4)=-0.25*(el15+el31);

akufel(8,1)=c3*el15-c2*el33;

akufel(8,2)=-c3*el15-c4*el33;

akufel(8,3)=-c1*el15+c4*el33;

akufel(8,4)=c1*el15+c2*el33;

i=1;

while i <= 8

j=1;

while j <= 4

akufel(i,j)=t*akufel(i,j);

j=j+1;

end

i=i+1;

end

con=c1*eps11+c2*eps33;

i=1;

while i <= 4

akffel(i,i)=con;

i=i+1;

end

akffel(1,2)=-c1*eps11+c4*eps33;

akffel(1,3)=-c3*eps11-c4*eps33;

akffel(1,4)=c3*eps11-c2*eps33;

akffel(2,3)=c3*eps11-c2*eps33;
```

```
akffel(2,4)=-c3*eps11-c4*eps33;

akffel(3,4)=-c1*eps11+c4*eps33;

akffel(2,1)=akffel(1,2);

akffel(3,1)=akffel(1,3);

akffel(4,1)=akffel(1,4);

akffel(3,2)=akffel(2,3);

akffel(4,2)=akffel(2,4);

akffel(4,3)=akffel(3,4);

i=1;

while i <= 4

j=1;

while j <= 4

akffel(i,j)=t*akffel(i,j);

j=j+1;

end

i=i+1;

end
```

NOMENCLATURE

D	vector of electrical displacement (charge per unit area)
$\boldsymbol{T}$	stress vector
$\boldsymbol{S}$	strain vector
$\boldsymbol{E}$	vector of the electric field
e	piezoelectric constant matrix
ε	dielectric matrix at constant strain
c	elasticity matrix at constant electric field
L	differential operator
u	displacement vector
ϕ	electrical potential
H	energy density
P_b, P_s, P_c	vectors of body, surface and concentrated forces
T	kinetic energy
ρ	mass density
$\dot{u}$	velocity vector
N	shape functions
F	applied force vector
G	applied charge vector
c_p	piezoelectric material capacitance
C_{uu}	proportional damping matrix
α, β	Rayleigh's coefficients

K	constant feedback gain matrix
D_f , D_v	position matrices for the force and voltage
A, B, C, D	state space matrices
v_{el}	transverse displacement
Q , R	state and input weighting matrices
S_c	solution for the algebraic Riccati equation

REFERENCES

1. M. P. Bayon and S. V. Hanagud, “Single Actuator and Multi-Mode Acceleration Feedback Control”, Georgia Institute of Technology, School of Aerospace Engineering, Atlanta Georgia, 1997.

2. U. Gabbert, T. Nestorovic Trajkov and H. Koppe, “Modelling, Control and Simulation of Piezoelectric Smart Structures using Finite Element Method and Optimal LQ Control”, *Mechanics, Automatic Control and Robotics*, Vol. 3, 2002, pp. 417-430.

3. K.-H. Rew, S. Kim, I. Lee and Y. Park, “Real-time estimations of multimodal frequencies for smart structures”, *Smart Materials and Structures*, 2002, pp. 36-47.

4. K. Kuhnen and H. Janocha, "Smart Piezoelectric Vibration Absorber", Saarland University, Laboratory for process Automation, 2001.

5. E. F. Crawley and J. de Luis, "Use of Piezoelectric Actuators as Elements of Intelligent Structures", *AIAA Journal*, Vol. 25, No. 10, 1987, pp. 1373-1385.

6. H. S. Tzou, "Development of a Light-Weight Robot End-Effector using a Polymeric Piezoelectric Bimorph", *IEEE International Conference on Robotics and Automation*, 1989.

7. Daryl L. Logan, "A First Course in the Finite Element Method", THOMSON LEARNING, Inc. 3rd edition, 2001.

8. Wodek K. Gawronski, "Advanced Structural Dynamics and Active Control of Structures", Springer, MECHANICAL ENGINEERING SERIES, 2004.

9. F. Hartmann, C. Katz, "Structural Analysis with Finite Element", Springer, 2004.

10. O. C. Zienkiewicz, R. L. Taylor, "The FINITE ELEMENT METHOD, Volume 2: SOLID MECHANICS", Butterworth Heinemann, 5th edition, 2003.

11. Tiersten H. F., "*Linear Piezoelectric Plate Vibrations*", Plenum Press, New York, 1969.

12. Mindlin, R. D., "Equations of High Frequency Vibrations of Thermopiezoelectric Crystal Plates", *International Journal of Solids & Structures*, Vol. 10, 1974, pp. 625-637.

13. www.morganmatroc.com

14. S. P. Timoshenko, J. N. Goddier, "Theory of Elasticity", McGraw-Hill, 1970.

15. Jon J. Thomsen, "Vibrations and Stability", Springer, 2003.

16. C. Jan, C. Hwang, "Robust Control Design for a Piezoelectric Actuator System with Dominant Hysteresis", IEEE, 2000, pp. 1515-1520.

17. A. J. Fleming, S. O. Moheimani, "Adaptive Piezoelectric Shunt Damping", Institute of Physics Publishing, Smart Materials and Structures, 2003, Vol. 12, pp. 36-48.

18. D. Halim, S. O. Moheimani, "Spatial H_2 Control of a Piezoelectric Laminate Beam: Experimental Implementation", IEEE, Vol.10, No. 4, 2002, pp. 533-546.

19. V. Giurgiutiu, "Active-Materials Induced-Strain Actuation for Aeroelastic Vibration Control", The Shock and Vibration Digest, Vol. 32, No. 5, 2000, pp. 355-368

20. World Book Encyclopedia, World Book Inc, Chicago, Vol. 15, 1992.

Khaled Al-Athel

Education

2002-2005 King Fahad University for Petroleum & Minerals
Dhahran, Saudi Arabia

Master Degree in Mechanical Engineering

- Worked in a funded research project under the name "Finite Element Analysis of Failure in Heat Transfer Line"
- Worked in a funded research project under the name "Simulation of a Computational Procedure for the Simulation of Laser Shock Processing"
- Degree is conferred with Second Honors

1997-2002 King Fahad University for Petroleum & Minerals
Dhahran, Saudi Arabia

Bachelor Degree of Science in Mechanical Engineering

- Degree is conferred with Third Honors

Professional activities

2002-2005 King Fahad University for Petroleum & Minerals
Dhahran, Saudi Arabia

Graduate Assistant at Mechanical Engineering Dept.

- Teaching senior level laboratory (System Dynamics & Control)
- TA for senior level course (Advanced Dynamics)